[American Journal of Science, Vol. 321, June, 2021, P. 643–679, DOI 10.2475/06.2021.01]

American Journal of Science

JUNE 2021

GEODYNAMIC ENVIRONMENT OF THE *CA.* 3800 MA OUTER ARC GROUP, ISUA (GREENLAND)

ALLEN P. NUTMAN*,**,†, CLARK R.L. FRIEND***, VICKIE C. BENNETT§, MARTIN VAN KRANENDONK**,§§,§§§, and ALLAN R. CHIVAS*,‡

ABSTRACT. **The arcuate, 35 km long Isua supracrustal belt (ISB, southern West Greenland) contains the world's largest remnants of Eoarchean volcanic and sedimentary sequences. The ISB is broadly divided into: (i) the northern *Inner Arc Group* of 3720 to 3690 Ma rocks, and (ii) the southern *Outer Arc Group* of *ca.* 3800 Ma rocks which is bounded on its northern side by the highly tectonized *ca.* 3750 Ma *Dividing Sedimentary Unit.* The boundary between the two groups is a mylonite formed between 3685 and 3660 Ma.**

Despite the generally high strain, amphibolite facies metamorphism and layer-parallel dislocations that can thin or altogether excise some units, domains of lower deformation comprising $\ll$1% (qualitative assessment) of the Outer Arc Group contain relict sedimentary and igneous structures. Combined with zircon U-Pb geochronology and whole rock geochemistry, this enables the Outer Arc Group lithological sequence and geodynamic setting to be reconstructed.

The lower part of the Outer Arc Group is dominated by metabasaltic amphibolites of the *Mafic Volcanic formation* in which rarely-preserved pillow structures indicate both their predominantly subaqueous eruption and also their stratigraphic facing. They erupted >3800 Ma, because they were first intruded by subconcordant sheets of fine-grained hypabyssal tonalite dated at 3803±3 Ma (Crowley, 2003) and then by coarser-grained 3795 to 3791 Ma tonalite-granodiorite, which forms a large deformed pluton along the south side of the ISB. This formation is succeeded by the *Sedimentary formation* whose base consists of discontinuous rare, thin fuchsitic quartzites with 3890 to 3805 Ma detrital zircons. Overlying is a diverse package of dolostones, marls and siliceous rocks. Although they are extensively modified by metamorphism and metasomatism, producing widespread growth of talc or tremolite, relict graded sedimentary layering, chemical and isotopic signatures indicate originally sedimentary protoliths. Detrital zircons in these rocks range in age from *ca.* 3820 to 3805 Ma. This unit shows an upwards transition from 'pure' chemical sedimentary rocks with distinct seawater-like trace element signatures into lithologies increasingly contaminated by felsic material that is locally preserved as graded layers, which are interpreted as an increasing volcanogenic input. Succeeding the sedimentary rocks is the *Felsic Volcanic formation*, an extensive unit of mostly schistose

* GeoQuEST Research Centre, School of Earth, Atmospheric and Life Sciences, University of Wollongong, Wollongong, NSW 2522, Australia

** Australian Centre for Astrobiology, University of New South Wales, Kensington, NSW 2052, Australia

*** Glendale, Tiddington, Oxon, OX9 2LQ, United Kingdom

§ Research School of Earth Sciences, Australian National University, Canberra, ACT 2601, Australia

§§ School of Biological, Earth and Environmental Sciences, University of New South Wales, Kensington, NSW 2052, Australia

§§§ Australian Research Council Centre of Excellence for Core to Crust Fluid Systems

‡ Department of Earth Sciences and Sprigg Geobiology Centre, The University of Adelaide, SA 5005, Australia

† Corresponding author: anutman@uow.edu.au

3807 to 3802 Ma felsic potassic-altered rocks with carbonate-rich interludes and veins. Locally-preserved andesitic units with graded layering, massive vesicular lavas, polymict breccias, resorbed quartz phenocrysts and fiammé, attest to volcanic and volcano-sedimentary protoliths. Whole rock geochemistry and oxygen isotope analyses on these rocks and their zircons indicate predominantly felsic volcanic protoliths that experienced massive alteration in a surficial environment, probably following subaerial eruption. Massive volcanic rocks are commonest in the west of the ISB, suggesting this part of the belt was proximal to a volcanic center.

Using these stratigraphic data, we conclude that the ISB volcanic and sedimentary rocks formed in a mobile geodynamic regime resembling plate tectonics, and not within a stagnant lid regime.

Key words: Isua supracrustal belt, Outer Arc Group, Eoarchean, stratigraphy, plate tectonics

INTRODUCTION

This contribution to a special issue of the American Journal of Science in honor of Alfred Kröner is on a topic that he pursued throughout his career; the interpretation of ancient metamorphic rocks. Our paper focusses on Eoarchean rocks (3600–4000 Ma), which are from the oldest part of the geological record for which diverse lithologies ranging from sedimentary rocks to mantle peridotites are preserved and have a known present-day global extent of only <20,000 km^2 (Nutman and others, 1996, 2013; S. Mojzsis written communication, 2021).

A key locality for unravelling Eoarchean processes is the Isua supracrustal belt (ISB) within the *Itsaq Gneiss Complex* of Greenland (fig. 1; Nutman and others, 1996; Friend and Nutman, 2019 and references therein). This is because the ISB is the world's largest preserved body (arcuate in outcrop and *ca.* 35 km long) of Eoarchean volcanic and sedimentary rocks, and consequently provides key information on early Earth's geodynamics, surficial processes and the emergence of life (see Nutman and Bennett 2018 and references therein for a recent summary). Geological mapping integrated with U-Pb zircon dating has demonstrated that the ISB contains juxtaposed slices of unrelated supracrustal rocks *ca.* 100 million years different in age (fig. 1; Nutman and others, 1993, 1996, 1997, 2002; Crowley and others, 2002; Crowley, 2003; Nutman and Friend, 2009). The belt's southern portion, which is the focus of this paper, consists of *ca.* 3800 Ma rocks and is informally named by us as the *Outer Arc Group* (Nutman and others, 2020). The belt's northern section comprises tectonic slices of *ca.* 3700 Ma rocks named the *Inner Arc Group* (fig. 1; Nutman and others, 1996, 1997, 2019, 2020; Nutman and Friend, 2009, and references therein). Recent publications have mostly focused on the *ca.* 3700 Ma Inner Arc Group, because of its greater diversity of preserved volcanic and sedimentary structures (Nutman and others 1984, 2017, 2019, Appel and others, 2009 and references therein). Use of the term 'arc' for both packages of rocks is a deliberate *double entendre*, to signify first the arcuate outcrop pattern of these units and secondly our contention they formed in environments geodynamically congruent with volcanic arcs.

In this paper, we focus on a reconstruction of the Outer Arc Group's *ca.* 3800 Ma succession. In the Discussion we compare its similarities and differences with the tectonically-juxtaposed Inner Arc Group and then explore whether the ISB volcanic and sedimentary rocks formed at convergent plate boundaries in a broadly uniformitarian geodynamic regime, or if they were the products of a postulated stagnant lid geodynamic regime proposed by some for the early Earth (for example, Webb and others, 2020).

ISUA SUPRACRUSTAL BELT

All Isua supracrustal belt (ISB) rocks have undergone poly-metamorphism with the maximum grade ranging from low amphibolite (500–550°C) to middle

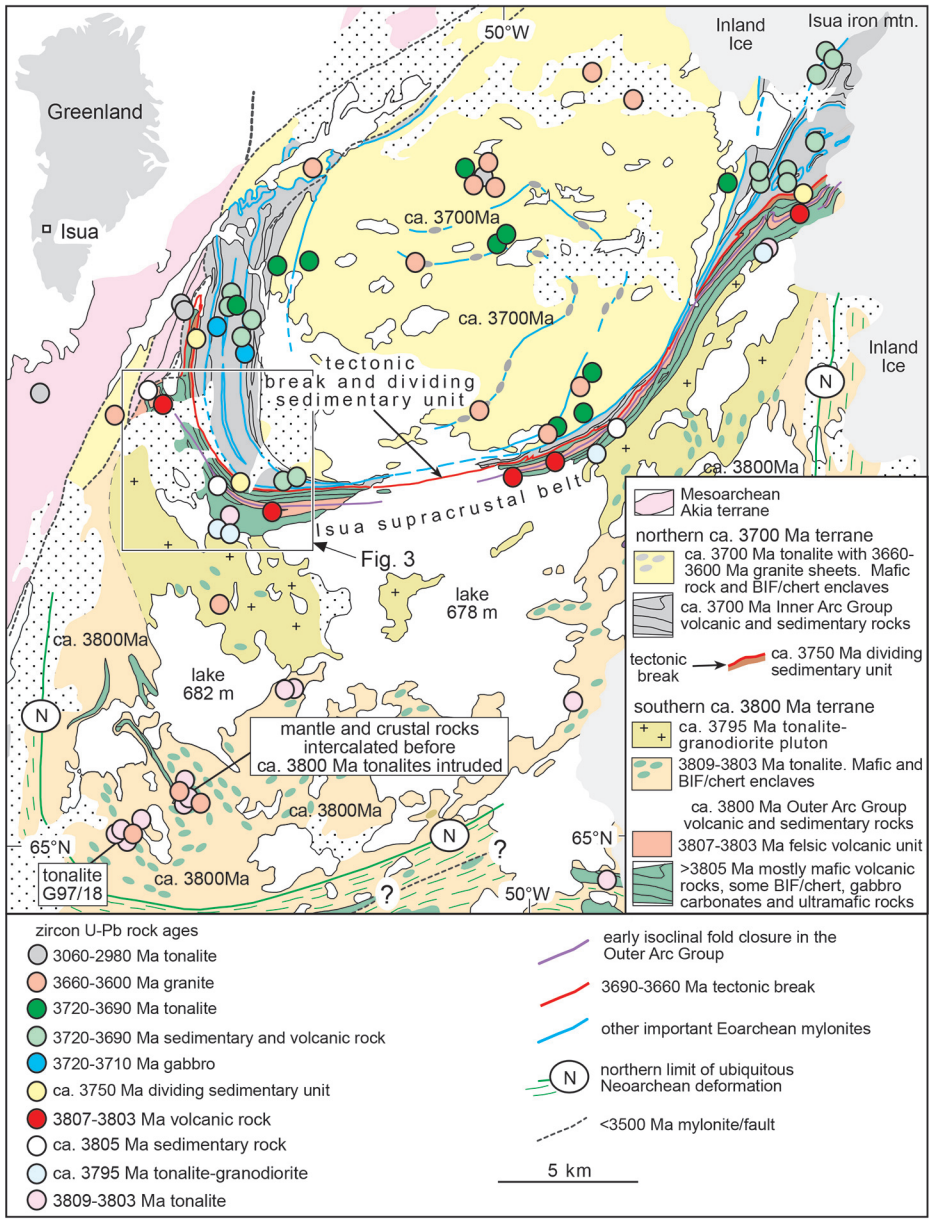

Fig. 1. Geological map of the northern end of the Itsaq Gneiss Complex (southern West Greenland).

amphibolite facies (up to 650°C), in different panels separated by Eoarchean mylonites (Boak and Dymek, 1982; Rollinson, 2003; Nutman and others, 2013). This is significantly lower metamorphic grade than much of the Itsaq Gneiss Complex, where Eoarchean upper amphibolite to granulite facies conditions were realized (Griffin and others, 1980; Nutman and others 1996; Friend and Nutman, 2005). Therefore, the ISB provides an important window onto the early Earth. The ISB is bounded by intrusive complexes, with most contacts tectonically modified (Bridgwater and

McGregor, 1974; Nutman and Friend, 2009). The intrusive complex to the south is dominated by *ca.* 3800 Ma tonalite protoliths and that to the north by *ca.* 3700 Ma tonalite protoliths invaded by copious 3650 to 3640 Ma granite sheets (Nutman and others, 1993, 1996, 1997, 2000; Crowley and others, 2002; Crowley, 2003; Nutman and Friend, 2009). To the west, the belt is in tectonic contact with Mesoarchean rocks, whilst eastwards it is obscured by the Inland Ice.

Primary volcanic and sedimentary structures have survived in only a few places, and the compositional layering in both the volcanic and sedimentary rocks is mostly of transposed tectonic origin (Nutman and others, 1984; Myers, 2001). The most common relict structures are pillows within mafic volcanic rocks, and more rarely, relict bedding which is found in cherts, banded iron-formation(BIF) and dolomite-rich rocks, together with graded bedding in felsic volcano-sedimentary rocks (for example, Nutman and others, 1984; 1997, 2007a, 2016, 2017; Komiya and others, 1999; Rosing, 1999; Solvang, 1999; Furnes and others, 2007).

THE OUTER ARC GROUP

Geological Mapping and Field Relationships

Figure 2 is a representation of the Outer Arc Group. From bottom to top (based on relict indicators of facing direction) here we informally divide the group into the Mafic Volcanic, Sedimentary and the Felsic Volcanic formations. We stress that figure 2 does not show a classic stratigraphic measured section, but instead schematically portrays lithological and age relationships, and the contrasts between the Outer Arc Group in the western and eastern parts of the ISB. Figure 3 is a geological map of the western end of the ISB, where the majority of rarely-preserved primary lithological features in the Outer Arc Group are found (location on fig. 1).

From the earliest investigations of the Isua supracrustal belt, lateral symmetry of lithologies was noted, including a median unit of felsic schists flanked by mafic rocks, peridotites and rocks of definite sedimentary origin such as magnetite-rich banded iron formation (fig. 1; for example, Keto and Kurki, 1967; Allaart, 1976). With the paucity of precise and accurate U-Pb zircon geochronology in the early 1980s (Baadsgaard, 1976; Baadsgaard and others, 1986a), a single stratigraphy was erected, which was recognized as being disrupted by early Archean tectonic breaks (Nutman and others, 1984). By the early 1990s however, with more accurate single grain U-Pb zircon geochronology, it was discovered that the belt is composite, with a northern *ca.* 3700 Ma portion and a southern *ca.* 3800 Ma portion (as termed here the Inner and Outer Arc Groups; Nutman and others, 1993, 1996, 2002, 2020; Nutman and Friend, 2009).

The median unit of felsic schist (3806±2 Ma; Compston and others, 1986) lies within what is here defined as the Outer Arc Group and is flanked on either side by carbonate-bearing and quartz-rich lithologies, then along much of its margins by an ultramafic schist unit, and then by amphibolites with thinner ultramafic schist and siliceous schist units. Strain in all these rocks is high, and it is only in exceptional circumstances (particularly in the hinge regions of folds) that primary igneous and sedimentary structures are preserved. In fact, fewer of these features are preserved than in the *ca.* 3700 Ma Inner Arc Group to the north.

In the outer flanking amphibolites, rarely-preserved pillow structures in metabasalts face upwards towards the median felsic schist unit (figs. 2 and 4A). This confirms that the median felsic schist unit is in an early isoclinal fold closure (Allaart, 1976; Nutman and others, 2002). Recently-discovered, relict, sedimentary and volcanic structures in the carbonate-bearing and quartz-rich lithologies in the Sedimentary and Felsic Volcanic formations yield consistent facing directions (fig. 2, and see below).

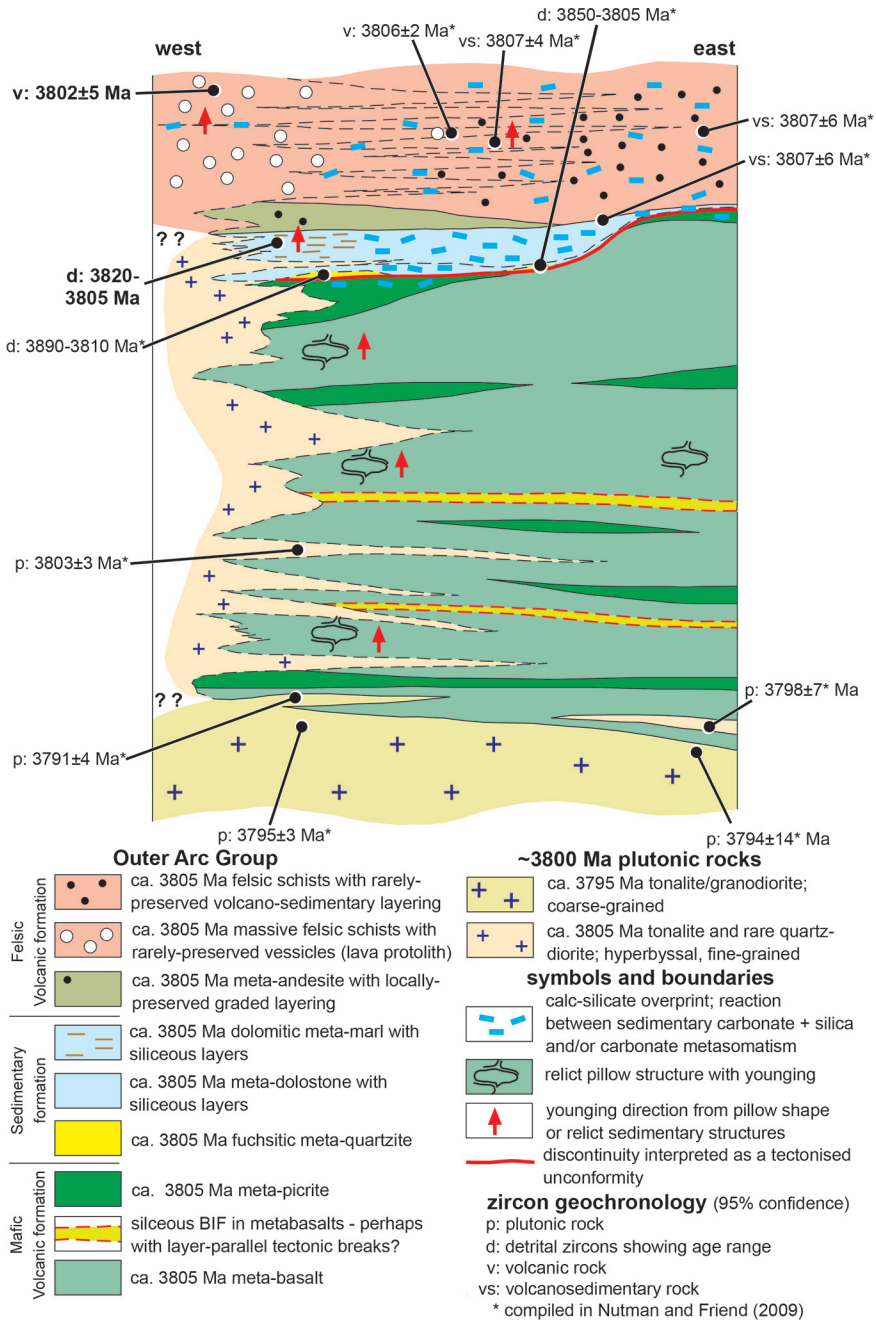

Fig. 2. Schematic section illustrating lithological sequence and geochronology for the Outer Arc Group of the Isua supracrustal belt.

Mafic Volcanic Formation

The base of this formation is not seen, but in the *ca.* 3800 Ma tonalites south of the ISB there are enclaves of similar amphibolites, layered gabbros and ultramafic rocks, indicating that a substantial lower part of it is missing from the ISB. This

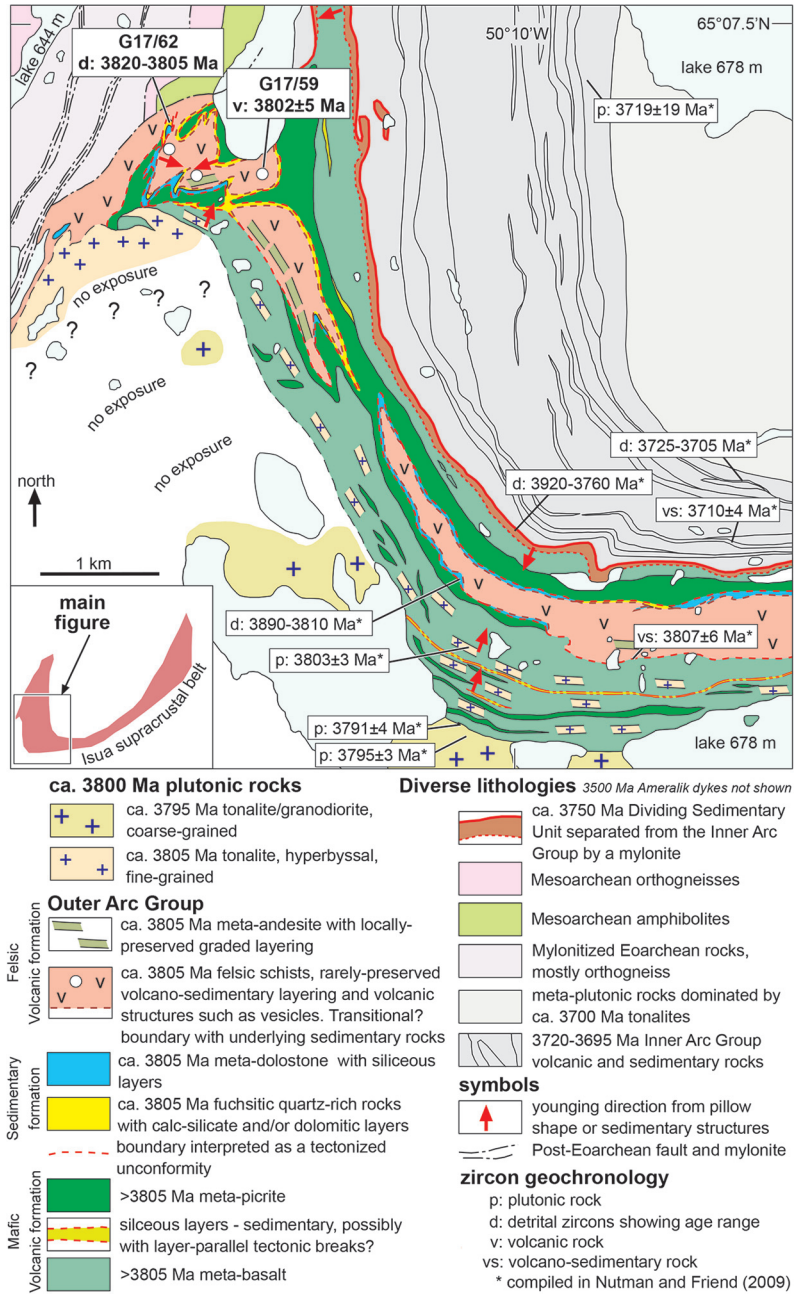

Fig. 3. Geological map of the western termination of the Isua supracrustal belt. This map is compiled from more detailed mapping undertaken in 1981 and 2017.

formation is composed of amphibolites with ultramafic schists and siliceous layers and is >3800 Ma because it is cut by discordant sheets of tonalite/granodiorite, that have U-Pb zircon ages of 3791±4 and 3803±3 Ma (figs. 2 and 3; Nutman and others, 1996; Crowley, 2003). The amphibolite mineralogy is predominantly hornblende + plagioclase ± quartz ± biotite, with only rare garnet. The rocks are devoid of felsic

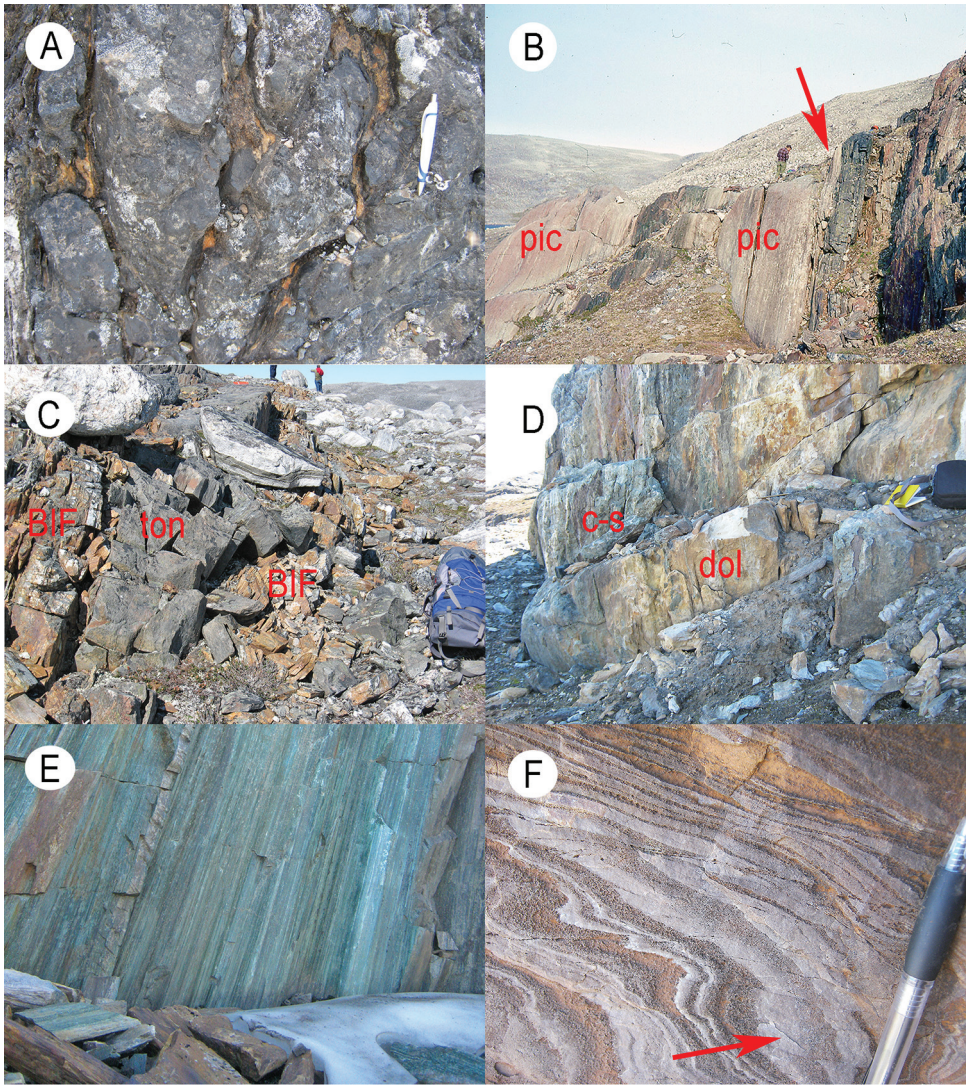

Fig. 4. Outcrop photographs of the Mafic Volcanic formation and the Sedimentary formation. (A) Example of basalt pillow structures, with carbonate-rich interstitial infill preserved within the Mafic Volcanic formation. Pen is 12 cm long. (B) Ultramafic schists of picritic composition with carbonate alteration at the top of the Mafic Volcanic formation. The arrow indicates the position of a thin fuchsite quartzite (sample G93/25) at the base of tectonically-thinned Sedimentary formation. Person for scale in the middle of the picture. (C) Thin siliceous banded iron formation horizon (*BIF*) within the Mafic Volcanic formation. It is intruded by a fine-grained tonalite sheet (*ton*), lithologically the same as one *ca.* 100 m to the north dated as 3803±3 Ma (Crowley, 2003). People for scale at top of the picture. (D) Best-preserved dolostone (*dol*) within the sedimentary formation. At 1 to 2 m to the left (labelled *c-s*), metamorphic reactions between quartz and dolomite layers have produced coarser-grained rocks rich in calc-silicates. Yellow A5 notebook for scale at right hand side of picture. (E) Rodded fuchsite-rich quartzites in a fold hinge. Unlike quartzite sample G93/25 (above), this rock did not yield zircons and is regarded as a deformed quartz vein. Field of view approximately 2 metres wide. (F) Very rare low-strain zone in the Sedimentary formation. Whilst showing small folds and the effects of minor displacements sub-parallel to the axial surfaces, quartz-rich layers grade into dolomite-bearing layers, across repeated cycles at this outcrop. Proposed facing direction is shown by the red arrow. Pen is 15 cm long.

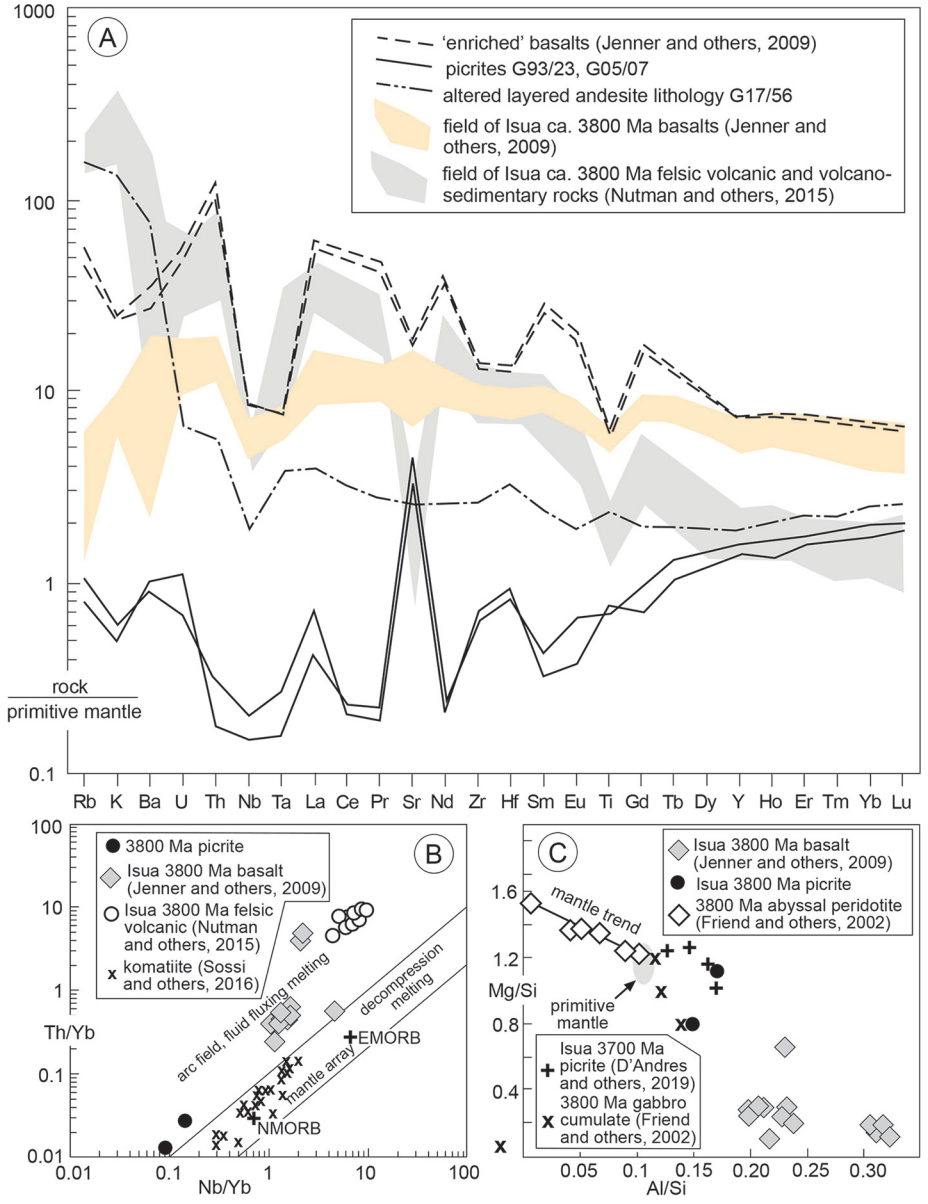

Fig. 5. Geochemistry of the Mafic Volcanic formation. (A) Primitive mantle (McDonough and Sun, 1995) normalized trace element plot using data of Jenner and others (2009). (B) Th/Yb – Nb/Yb plot. (C) Mg/Si – Al/Si (wt proportions) for the Mafic Volcanic formation rocks, in comparison with mantle peridotites and layered ultramafic cumulates from south of the Isua supracrustal belt (data from Friend and others, 2002).

segregations, indicating peak metamorphism at lower to middle amphibolite facies conditions. Based on sporadic preservation of pillow structures throughout (fig. 4A), the amphibolites are interpreted to have had predominantly subaqueous basalt protoliths (Nutman and others, 1984; Jenner and others, 2009). Detailed geochemical studies of these amphibolites by several researchers (table 1; Polat and Hofmann; 2003;

TABLE 1

Whole rock data

sample	G05/07	G93/23	JG03/39[a]	JG03/40a[a]	JG03/42[a]	JG03/63[a]	JG03/41[a]	JG03/43[a]	JG03/45[a]	JG03/46[a]	JG03/48[a]	JG03/49[a]	JG03/50[a]
lithology	ultramafic schist (picrite)	ultramafic schist (picrite)	high-Mg basalt	enriched	enriched	enriched	basalt	basalt	basalt	basalt	basalt	basalt	basalt
affinity	Mafic Volcanic fm.	Mafic Volcanic fm.	Mafic Volcanic fm.	Mafic Volcanic fm.	Mafic Volcanic fm.	Mafic Volcanic fm.	Mafic Volcanic fm.	Mafic Volcanic fm.	Mafic Volcanic fm.	Mafic Volcanic fm.	Mafic Volcanic fm.	Mafic Volcanic fm.	Mafic Volcanic fm.
age (Ma)	>3803	>3803	>3803	>3803	>3803	>3803	>3803	>3803	>3803	>3803	>3803	>3803	>3803
lat. (N)	65°09.84'		65°05.07'	65°05.11'	65°05.11'	65°05.09'	65°05.11'	65°05.11'	65°05.11'	65°05.11'	65°05.11'	65°05.11'	65°05.11'
long. (W)	49°48.91		50°10.45	50°10.47	50°10.47	50°10.41	50°10.46	50°10.46	50°10.46	50°10.46	50°10.46	50°10.46	50°10.46
SiO_2	39.68	43.57	42.4	47.3	49.6	51.3	51.4	53.1	52.7	50.8	51.7	51.2	52.6
TiO_2	0.10	0.09	0.53	0.94	0.94	0.97	0.99	1.01	0.97	0.87	0.76	0.75	0.77
Al_2O_3	5.97	5.71	8.6	13.2	13.5	10.3	14.6	14.5	14.5	9.2	9.3	9.3	9.5
Fe_2O_3	10.28	8.60	13.2	11.2	11.5	14.3	11.4	12.3	11.5	13.6	13	12.9	12.2
FeO													
MnO	0.17	0.14	0.21	0.24	0.23	0.22	0.19	0.17	0.21	0.22	0.22	0.22	0.21
MgO	34.34	27.06	21.4	7.3	7	9.7	5	5.2	5.3	12	11.4	11.4	10.9
CaO	1.77	5.51	8.4	11.1	10	9.8	7	6.5	8	10.6	10.6	10.7	10.8
Na_2O	0.09	0.15	0.47	3.79	3.98	2.78	5.18	4.27	4.67	1.61	1.77	1.81	2.14
K_2O	0.01	0.01	0.03	0.58	0.55	0.19	0.25	1.15	0.13	0.16	0.16	0.16	0.16
P_2O_5	0.01	0.01	0.05	0.41	0.33	0.12	0.1	0.1	0.1	0.05	0.05	0.05	0.05
LOI	6.94	8.74											
SO_3	0.04	0.01											
total	99.40	99.59	95.4	96	97.6	99.7	98.8	98.2	98.1	99	98.9	98.6	99.3
trace elements													
Cr			1825	285	234	557	80	63	83	974	960	986	975
Ni	1731	1419	685	86.6	76.1	340	69.8	60	70.7	257	250	258	244
V													
Rb	0.42	0.32	0.35	30.24	23.22	1.06	3.79	40.05	0.53	1.43	1.52	1.49	1.13
Sr	48.7	66.2	35.4	300	282	492	229	178	265	101	122	127	173
Ba	3.94	4.43	2	195	148	108.3	52.9	219	11.5	41	45.3	41.8	49.5
Y	4.10	4.64	12.1	23.9	23.2	15	21.7	23.7	21.2	16.3	15.9	15.8	15.8
Nb	0.08	0.06	1.46	4.41	4.05	6.43	3.73	3.83	3.54	2.35	2.33	2.27	2.42
Zr	4.84	4.23	28.1	120	111	79.4	90.4	94.5	87.3	65.2	63.7	62.4	64.5
Hf	0.18	0.16	0.84	3.17	2.92	1.97	2.39	2.48	2.33	1.76	1.72	1.69	1.78
Ta	0.01	0.00	0.1	0.23	0.22	0.4	0.25	0.26	0.24	0.17	0.16	0.17	0.17
Pb													
Th	0.02	0.01	0.32	9.17	7.74	0.72	1.28	1.33	1.22	0.95	0.92	0.89	0.94
U	0.01	0.01	0.1	0.98	0.84	0.15	0.3	0.32	0.26	0.19	0.19	0.19	0.2
La	0.30	0.17	2.74	35.8	31.4	18.6	7.79	8.72	8.29	4.74	4.29	4.64	4.64
Ce	0.20	0.23	6.27	81.9	71.2	44.3	19.7	21.3	19.9	12.5	11.6	12.1	12.2
Pr	0.03	0.03	1.04	10.85	9.42	5.84	2.82	3.01	2.79	1.85	1.75	1.8	1.81
Nd	0.16	0.19	5.09	46.6	40.8	24.4	13	13.8	12.9	9.03	8.52	8.82	8.76
Sm	0.08	0.11	1.57	10.14	8.87	4.55	3.53	3.69	3.39	2.7	2.6	2.6	2.63
Eu	0.04	0.07	0.67	2.67	2.34	1.32	1.13	1.13	1.09	0.89	0.88	0.88	0.83
Gd	0.26	0.35	2	8.19	7.43	3.97	4.11	4.3	3.97	3.25	3.2	3.17	3.15
Tb	0.07	0.09	0.37	1.07	1.02	0.59	0.7	0.75	0.68	0.57	0.55	0.55	0.56
Dy	0.56	0.69	2.24	5.11	4.91	3.1	4.19	4.43	3.96	3.23	3.19	3.14	3.23
Ho	0.14	0.17	0.47	0.91	0.89	0.59	0.85	0.92	0.81	0.64	0.64	0.63	0.63
Er	0.50	0.55	1.35	2.37	2.34	1.6	2.45	2.65	2.36	1.83	1.77	1.7	1.77
Tm													
Yb	0.56	0.65	1.32	2.04	2.02	1.37	2.29	2.46	2.26	1.58	1.55	1.58	1.57
Lu	0.09	0.10	0.19	0.28	0.28	0.2	0.34	0.36	0.32	0.23	0.23	0.22	0.22
methods	XRF-GA ICP-ANU	XRF-GA ICP-ANU	XRF-GA ICP-ANU	XRF-GA ICP-ANU	XRF-GA ICP-ANU	XRF-GA ICP-ANU	XRF-GA ICP-ANU	XRF-GA ICP-ANU	XRF-GA ICP-ANU	XRF-GA ICP-ANU	XRF-GA ICP-ANU	XRF-GA ICP-ANU	XRF-GA ICP-ANU

TABLE 1
(continued)

sample	JG03/52[a]	JG03/53[a]	JG03/54[a]	JG03/55[a]	JG03/57[a]	JG03/60[a]	JG03/62[a]	JG03/64[a]	170728[b]	G17/40	G17/40	G12/84	G17/55
lithology	basalt	basalt	basalt	basalt	basalt	basalt	basalt	basalt	dolostone	dolostone whole rock	carbonate analysis	carbonate analysis	carbonate analysis
affinity	Mafic Volcanic fm.	Mafic Volcanic fm.	Mafic Volcanic fm.	Mafic Volcanic fm.	Mafic Volcanic fm.	Mafic Volcanic fm.	Mafic Volcanic fm.	Mafic Volcanic fm.	Mafic Volcanic fm.	Sedimentary fm.	Sedimentary fm.	Sedimentary fm.	Sedimentary fm
age (Ma)	>3803	>3803	>3803	>3803	>3803	>3803	>3803	>3803	ca. 3805	ca. 3805	ca. 3805	ca. 3805	ca. 3805
lat. (N)	65°05.11'	65°05.11'	65°05.11'	65°05.11'	65°05.11'	65°05.10'	65°05.10'	65°05.18'	65°05.45'	65°05.45'	65°05.45'	65°05.45'	65°05.45'
long. (W)	50°10.46	50°10.46	50°10.46	50°10.46	50°10.46	50°10.37	50°10.38	50°10.67	50°07.04	50°07.04	50°07.04	50°07.04	50°07.04
SiO_2	51.1	51.3	51.3	52.8	53.1	59	47.7	52.5	3.19				
TiO_2	0.78	0.74	0.76	0.77	0.89	0.8	0.97	0.74	0.02				
Al_2O_3	9.4	9.5	9	9.3	11.1	11.3	9.7	9.3	0.04				
Fe_2O_3	13.3	13.2	12.3	12.6	12.4	9	16.3	12	0.06				
FeO									3.47				
MnO	0.22	0.22	0.22	0.21	0.25	0.15	0.29	0.21	0.24				
MgO	11.5	11.4	10.8	11.2	8.3	4.9	10.5	12.1	22.84				
CaO	10.4	10.6	11.2	10.5	8.9	9.1	9.8	9.9	23.51				
Na_2O	1.84	1.9	1.71	1.68	3.43	3.5	2.07	1.59	<0.01				
K_2O	0.21	0.22	0.16	0.16	0.16	0.15	0.18	0.21	0.01				
P_2O_5	0.05	0.05	0.05	0.05	0.06	0.05	0.06	0.05	n.d.				
LOI									44.95				
SO_3													
total	98.8	99.1	97.6	99.3	98.6	98	97.5	98.6	98.33				
trace elements													
Cr	994	921	915	929	276	231	316	1094	24	5			
Ni	256	244	228	240	99.2	73.7	273	326	n.d.	20.3		13.0	
V										4		0.53	
Rb	2.77	2.83	1.32	1.05	1.18	0.96	0.76	2.58	0.7	0.09			
Sr	138	161	140	135	193	222	70.1	154	141	65.1			
Ba	66.2	76.1	43.5	41.3	37	34.8	10.4	53.3	14	20			
Y	16.9	16.4	15.9	15.7	18.6	18.5	19.3	15.6	11.6	6.8	9.38	2.02	2.70
Nb	2.31	2.22	2.42	2.28	2.46	2.27	2.49	2.39	0.21	0.09			
Zr	65.3	62.5	63.8	64.9	69.4	62.5	75.2	64.8	0.8	0.4			
Hf	1.79	1.63	1.69	1.72	1.88	1.68	2.01	1.73	0.2	0.09			
Ta	0.17	0.16	0.16	0.17	0.17	0.16	0.18	0.17	0.03	0.04			
Pb										35.1			
Th	0.94	0.87	0.9	0.9	0.83	0.74	0.87	0.97	0.07	0.09		0.00	
U	0.22	0.21	0.19	0.19	0.18	0.18	0.18	0.21	0.03	0.09		0.00	
La	5.04	5.74	4.7	4.65	4.71	6.39	4.02	6.13	2	2.2	0.75	1.00	1.43
Ce	13	14.2	12	11.5	12.2	15.2	11.1	15	2.84	2.44	0.82	0.86	2.57
Pr	1.93	2.03	1.77	1.73	1.85	2.18	1.73	2.14	0.46	0.26	0.10	0.09	0.33
Nd	9.46	9.73	8.61	8.37	9.31	10.6	8.84	10.1	1.97	1.1	0.48	0.35	1.38
Sm	2.84	2.77	2.56	2.54	2.9	2.94	2.8	2.73	0.67	0.25	0.17	0.09	0.35
Eu	0.95	0.95	1.02	0.8	0.88	1.2	1.03	0.87	0.56	0.23	0.27	0.11	0.28
Gd	3.41	3.26	3.07	3.09	3.58	3.66	3.58	3.18	0.81	0.41	0.42	0.14	0.46
Tb	0.59	0.56	0.54	0.54	0.63	0.61	0.63	0.53	0.11	0.05	0.07	0.02	0.07
Dy	3.37	3.21	3.1	3.07	3.63	3.57	3.72	3.06	0.89	0.4	0.54	0.10	0.38
Ho	0.68	0.62	0.61	0.61	0.73	0.7	0.75	0.61	0.21	0.11	0.14	0.03	0.07
Er	1.86	1.73	1.72	1.7	2.04	1.98	2.13	1.7	0.58	0.3	0.42	0.07	0.18
Tm										0.04	0.06	0.01	0.02
Yb	1.66	1.55	1.54	1.5	1.83	1.72	1.91	1.52	0.56	0.29	0.40	0.06	0.15
Lu	0.24	0.22	0.22	0.21	0.27	0.25	0.27	0.22	0.09	0.04	0.06	0.01	0.02
methods	XRF-GA ICP-ANU	XRF-GA ICP-ANU	XRF-GA ICP-ANU	XRF-GA ICP-ANU	XRF-GA ICP-ANU	XRF-GA ICP-ANU	XRF-GA ICP-ANU	XRF-GA ICP-ANU	XRF-Cph ICP-ANU	XRF-UOW ICP-ALS	ICP-ANU	ICP-ANU	ICP-ANU

TABLE 1
(continued)

sample	G17/47	G17/49	G17/44	G17/52A	G17/52B	G17/56	G17/59	G17/66	G93/24[c]	G04/68[c]	G04/69[c]	248203[c]	G11/78[c]
lithology	dolostone	dolostone	layered sediment	layered sediment	layered sediment	felsic schist	felsic schist	felsic schist	felsic schist	felsic schist	felsic schist	felsic schist clast	felsic schist matrix
affinity	Sedimentary fm.	Sedimentary fm.	Sedimentary fm.	Sedimentary fm.	Sedimentary fm.	Felsic Volcanic fm.	Felsic Volcanic fm.	Felsic Volcanic fm.	Felsic Volcanic fm.	Felsic Volcanic fm.	Felsic Volcanic fm.	Felsic Volcanic fm.	Felsic Volcanic fm.
age (Ma)	ca. 3805	ca. 3805	ca. 3805	ca. 3805	ca. 3805	ca. 3805	3802±5	ca. 3805	ca. 3805	ca. 3805	ca. 3805	3806±2	ca. 3805
lat. (N)	65°06.89'	65°06.89'	65°07.13'	65°07.00'	65°07.00'	65°06.90'	65°06.97'	65°06.97'		65°09.46'	65°09.46'	65°05.76'	65°05.76'
long. (W)	50°13.03	50°13.03	50°13.07	50°12.78	50°12.78	50°12.75	50°12.23	50°12.23		49°49.96	49°49.96	50°00.39	50°00.39
SiO_2	21.44	38.24	74.59	55.32	28.29	51.48	62.7	64.69	62.58	66.45	66.71	68.92	49.57
TiO_2	0.19	0.16	0.01	0.07	0.07	0.34	0.47	0.51	0.56	0.45	0.55	0.44	0.26
Al_2O_3	4.55	3.8	0.39	1.16	1.87	18.18	15.4	16.44	15.99	14.83	15.24	15.30	8.73
Fe_2O_3	11.96	10.59	6.61	5.91	9.27	9.25	4.7	3.4	4.62	3.32	3.35	0.69	5.69
FeO													
MnO	0.6	0.39	0.32	0.44	0.73	0.1	0.18	0.08	0.08	0.14	0.16	0.02	0.39
MgO	9.61	7.38	3.26	5.64	8.99	10.99	2.58	1.41	2.10	2.19	1.89	0.69	4.61
CaO	19.82	15.47	8.06	12.38	19.83	3.02	5.31	2.68	4.47	4.48	3.83	0.84	11.91
Na_2O	0.55	0.24	< 0.020	0.09	0.45	0.54	0.26	0.25	0.27	0.12	0.19	0.58	0.18
K_2O	1.23	0.96	0.01	0.32	0.36	3.57	8.05	9.23	5.76	4.71	5.42	11.09	4.64
P_2O_5	0.05	0.03	0.01	0.02	0.05	0.02	0.16	0.15	0.22	0.14	0.15	0.18	0.11
LOI	28.85	22.08	6.35	17.99	29.53	2.33	0	1.02	3.13	3.06	2.40	1.03	12.06
SO_3	0.44	0.19	0.31	0.32	0.33	0.01	0.02	0.02					
total	99.29	99.54	99.93	99.66	99.76	99.83	99.82	99.86	99.76	99.87	99.90	99.78	98.16
trace elements													
Cr	1450	1290	153	692	611	190	118	77	56.0	47.0	57.2	29.5	47.2
Ni	2000	1080	98.5	260	386	228	25.9	23.8					12.3
V	81	68	5	25	28	189	53	56	69.4	57.8	61.3	43.2	
Rb	35.1	32.3	0.3	7.4	9	88.5	122	141	132	95	100	116	88
Sr	61.7	30.9	24	9.4	15.6	36.3	64.4	36.3	46.0	30.1	21.1	18.1	24.19
Ba	280	90	9	80	120	450	550	420	505	63.5	42.4	1230	652
Y	5.7	5.3	2.2	1.6	2.6	5.6	10.2	10.4	10.7	8.13	9.27	5.48	5.53
Nb	3.1	0.8	0.4	0.2	0.1	0.9	5.3	5.5	4.90	4.35	4.41	4.71	2.63
Zr	9.8	6.3	2	3.1	3.3	19.9	136.5	160	146	118	110	138	73.9
Hf	0.3	0.2	0.1	0.1	0.1	0.7	3.7	4.4	3.79	2.94	2.77	3.52	2.05
Ta	0.17	0.07	0.04	0.04	0.04	0.11	0.35	0.37	0.88	1.22	0.62	1.34	0.29
Pb	17.8	13.5	1.2	532	17.9	22.6	19.3	17.3					7.83
Th	0.27	0.08	0.05	0.02	0.06	0.34	5.57	6.53	7.13	4.93	4.65	4.79	2.68
U	0.1	0.09	0.09	0.09	0.09	0.1	1	1.2	1.31	0.71	0.63	0.66	0.527
La	2.7	1	0.5	0.5	0.7	1.9	31	33.4	33.2	23.1	24.2	28.6	19.6
Ce	5.22	2.12	0.97	0.53	1.61	3.87	64.1	70	70.7	49.0	50.4	63.3	36.1
Pr	0.69	0.31	0.14	0.07	0.24	0.51	7.69	8.14	8.65	5.74	5.90	7.48	3.98
Nd	3.3	1.6	0.6	0.4	1.2	2.4	29.1	30.5	33.2	21.7	22.5	26.8	15.9
Sm	0.84	0.52	0.16	0.13	0.32	0.7	4.33	4.47	5.60	3.69	3.77	4.23	2.59
Eu	0.41	0.22	0.09	0.08	0.11	0.21	1.09	1.03	1.34	0.94	0.96	0.77	0.69
Gd	1.00	0.73	0.23	0.19	0.38	0.78	3.01	3.08	3.51	2.51	2.54	2.24	1.4
Tb	0.15	0.13	0.04	0.03	0.06	0.14	0.36	0.38	0.47	0.36	0.37	0.29	0.21
Dy	0.97	0.81	0.25	0.22	0.38	0.91	1.94	2.11	2.34	1.71	1.99	1.20	1.04
Ho	0.2	0.18	0.06	0.05	0.08	0.22	0.35	0.36	0.41	0.31	0.37	0.19	0.23
Er	0.54	0.52	0.18	0.16	0.23	0.71	0.97	0.95	1.01	0.74	0.90	0.56	0.48
Tm	0.08	0.07	0.03	0.02	0.03	0.11	0.14	0.14					0.07
Yb	0.47	0.47	0.19	0.14	0.25	0.83	0.87	0.9	0.92	0.55	1.02	0.52	0.42
Lu	0.07	0.06	0.03	0.02	0.03	0.13	0.12	0.14	0.13	0.08	0.16	0.08	0.05
methods	XRF-UOW ICP-ALS	XRF-UOW ICP-ALS	XRF-UOW ICP-ALS	XRF-UOW ICP-ALS	XRF-UOW ICP-ALS	XRF-UOW ICP-ALS	XRF-UOW ICP-ALS	XRF-UOW ICP-ALS	XRF-GA ICP-ANU	XRF-GA ICP-ANU	XRF-GA ICP-ANU	XRF-Cph ICP-ANU	XRF-GA ICP-ANU

TABLE 1
(continued)

sample	G11/79[c]	G11/76[c]	G11/77[c]	G97/102	229461	229464	225951	225937	229459	225932	292128[d]	G97/18[d]	G97/38[d]
lithology	felsic schist matrix	felsic schist clast	felsic schist clast	felsic schist	hypabyssal tonalite	hypabyssal tonalite	hypabyssal tonalite	hypabyssal tonalite	hypabyssal tonalite	hypabyssal tonalite	southern quartz diorite	southern tonalite	southern tonalite
affinity	Felsic Volcanic fm.	Felsic Volcanic fm.	Felsic Volcanic fm	Felsic Volcanic fm.	intrusion	intrusion	intrusion	intrusion	intrusion	intrusion	intrusion	intrusion	intrusion
age (Ma)	ca. 3805	ca. 3805	ca. 3805	3807±6	ca. 3803	ca. 3803	ca. 3803	ca. 3803	ca. 3803	ca. 3803	3806±5	3808±4	3811±6
lat. (N)	65°05.76'	65°05.76'	65°05.76'	65°05.18'								65°00.63'	65°00.63'
long. (W)	50°00.39	50°00.39	50°00.39	50°09.23								50°15.04	50°15.04
SiO_2	47.39	62.34	61.25		67.12	65.49	67.15	65.6	66.59	64.69	54.73	69.79	70.13
TiO_2	0.26	0.46	0.40		0.44	0.46	0.42	0.44	0.44	0.45	0.91	0.25	0.25
Al_2O_3	8.48	15.49	12.86		15.69	15.18	15.45	15.53	15.84	15.37	19.1	16.7	16.74
Fe_2O_3	6.32	1.08	3.00		0.39	0.52	0.4	0.77	0.56	0.77	7.16	2.12	2.05
FeO					2.27	3.16	2.8	2.54	2.66	2.88			
MnO	0.43	0.07	0.15		0.04	0.06	0.03	0.07	0.06	0.09	0.1	0.03	0.03
MgO	5.08	0.68	1.88		1.39	1.69	1.38	1.43	1.39	1.53	3.37	0.94	0.89
CaO	12.90	3.16	5.04		3.45	3.71	3.58	3.62	3.56	3.81	7.71	3.94	3.93
Na_2O	0.29	0.47	0.15		3.6	3.48	4.7	3.5	3.93	3.75	4.87	5.22	5.33
K_2O	4.63	11.46	7.16		1.08	1.81	1.58	2.45	2.34	2.41	1.28	0.93	0.98
P_2O_5	0.11	0.23	0.15		0.12	0.14	0.13	0.13	0.13	0.14	0.29	0.08	0.07
LOI	13.49	3.36	5.61		2.34	2.91	1.72	3.73	2.29	3.04			
SO_3											0.19	0.01	0.01
total	99.37	98.81	97.64		97.92	98.61	99.34	99.81	99.81	98.93	99.81	100.07	100.46
trace elements													
Cr	42.8	69	42.5	80	25	59	22	24	19	32			
Ni	9.9	11.4	10.4		12	26	11	13	10	11	44	17	15
V				40	47	55	46	45	49	46	115	21	19
Rb	105	120	99.4	85.1	30	49	67	64	57	69	35	31	37
Sr	31.5	15.4	16.4	65.9	351	343	399	301	256	269	642	429	431
Ba	540	599	971	221	307	392	453	323	361	341	163	100	122
Y	6.35	8.08	6.39	5.9	13	12	14	11	10	12	18.2	2.9	3
Nb	3.01	4.92	3.7	4.4	4	6	6	6	5	3	5.6	1.3	1.3
Zr	80.5	116	103	139	145	142	130	121	115	120	54	121	125
Hf	2.23	3.06	2.84	3.6							1.8	3.2	3.4
Ta	0.324	0.50	0.46	0.4							0.51	0.21	0.2
Pb	9.62	15.7	12.2	600	17	13	10	17	17	15	15.2	6.5	9
Th	3.15	4.29	3.6	5.43	5	8	8	9	7	8	1.31	0.77	0.79
U	0.656	1.40	0.70	1.42							1.05	0.32	0.33
La	22.6	32.2	25.8	18.1							20.2	5.81	5.17
Ce	43.4	61.3	49	35							53.6	11.4	10.3
Pr	4.74	6.77	5.28	4.08							8.29	1.48	1.31
Nd	18.3	27	21.2	14.8							37.4	6.05	5.89
Sm	2.9	4.13	3.28	2.35							7.41	1.3	1.38
Eu	0.83	0.96	0.88	0.52							1.94	0.48	0.45
Gd	1.97	2.43	1.97	1.61							5.19	0.91	0.98
Tb	0.22	0.33	0.30	0.21							0.66	0.13	0.19
Dy	1.23	1.46	1.26	0.96							3.63	0.63	0.56
Ho	0.25	0.29	0.22	0.21							0.68	0.12	0.1
Er	0.56	0.69	0.61	0.63							1.74	0.27	0.26
Tm	0.07	0.12	0.09	0.09									
Yb	0.53	0.61	0.56	0.62							1.52	0.28	0.3
Lu	0.06	0.10	0.07	0.09							0.2	0.039	0.035
methods	XRF-GA ICP-ANU	XRF-GA ICP-ANU	XRF-GA ICP-ANU	XRF-GA ICP-ANU	XRF-Cph	XRF-Cph	XRF-Cph	XRF-Cph	XRF-Cph	XRF-Cph	XRF-GA ICP-ANU	XRF-GA ICP-ANU	XRF-GA ICP-ANU

TABLE 1
(continued)

sample	G97/31[d]	G93/44[d]	G97/97[d]	G97/98[d]	225943	225841	225909
lithology	southern tonalite	southern tonalite	southern granodiorite	southern granodiorite	southern granodiorite	southern granodiorite	southern granodiorite
affinity	intrusion	intrusion	intrusion	intrusion	intrusion	intrusion	intrusion
age (Ma)	3809±8	3806±8	ca. 3795	3795±3	ca. 3795	ca. 3795	ca. 3795
lat. (N)	65°00.75'		65°04.89'	65°04.89'			
long. (W)	50°13.08		50°10.66	50°10.66			
SiO_2	66.79	70.02	71.75	69.23	70.69	68.04	71.47
TiO_2	0.31	0.27	0.3	0.33	0.32	0.38	0.26
Al_2O_3	17.93	16.45	15.1	16.19	15.75	15.27	14.9
Fe_2O_3	2.36	1.95	2.47	2.61	0.43	1.31	0.29
FeO					1.87	1.74	1.69
MnO	0.03	0.02	0.04	0.05	0.03	0.05	0.04
MgO	1.2	0.96	0.71	0.96	0.71	1.45	0.63
CaO	5.02	3.57	2.82	3.44	3.11	3.35	2.52
Na_2O	5.4	5.14	4.73	4.89	5.03	4.28	4.71
K_2O	0.79	1.08	1.86	1.66	1.23	2.24	2.27
P_2O_5	0.07	0.08	0.01	0.01	0.1	0.13	0.08
LOI					0.59	1.66	0.66
SO_3	0.01	0.05	0.08	0.09			
total	100.00	99.66	99.86	99.53	99.86	99.81	99.52
trace elements							
Cr					10	30	16
Ni	18	12	12	17	2	16	5
V	26	19	17	22	18	39	18
Rb	26	53	78	72	51	73	71
Sr	469	394	236	294	483	466	258
Ba	87	136	212	204	399	520	331
Y	3.5	1.4	8.6	16.3	6	13	9
Nb	1.2	1.6	4.3	3.8	7	7	6
Zr	115	109	124	86	180	108	103
Hf	2.9	3	3.6	2.7			
Ta	0.16	0.26	0.45	0.81			
Pb	10.3	12	13.9	15.1	16	16	18
Th	4.83	4.23	21.6	15			
U	9.8	7.7	41.1	25			
La	1.38	0.9	4.68	3.34			
Ce	6.18	3.37	16.6	13.5			
Pr	1.23	0.64	2.81	2.92			
Nd	0.54	0.37	0.74	0.65			
Sm	1.14	0.47	1.93	2.79			
Eu	0.15	0.05	0.28	0.39			
Gd	0.75	0.29	1.58	2.86			
Tb	0.11	0.06	0.29	0.54			
Dy	0.3	0.15	0.92	1.58			
Ho							
Er	0.29	0.17	0.88	1.62			
Tm	0.045	0.027	0.13	0.25			
Yb	4.83	4.23	21.6	15			
Lu	9.8	7.7	41.1	25			
methods	XRF-GA ICP-ANU	XRF-GA ICP-ANU	XRF-GA ICP-ANU	XRF-GA ICP-ANU	XRF-Cph	XRF-Cph	XRF-Cph

GPS positions according to the WGS84 datum. Samples without GPS positions were collected 1974-1993.

Methods: XRF-GA = XRF at Geoscience Australia; ICP-ANU = ICPMS at the Australian National University; XRF-Cph = XRF at the Geoscience Institute, Copenhagen; NA-Risø = Neutron activation at the Risø reactor facility, Denmark; XRF-UOW = XRF at the University of Wollongong; ICP-ALS = ICP at ALS (Brisbane).

a from Jenner and others (2009); b from Nutman and others (2010), c from Nutman and others (2015), d from Nutman and others (1999).

Jenner and others, 2009; Hoffmann and others, 2011a) have revealed an enrichment of the light rare earth elements (REE) versus the heavy REE and the presence of distinct negative Ti, Nb and Ta anomalies in primitive mantle-normalized trace element plots (fig. 5A; using data of Jenner and others, 2009).

The associated ultramafic schist units have been much less studied. This is because the most prominent unit near the structural (and stratigraphic) top of the formation has been largely metasomatized/altered, including carbonate and calc-silicate veins that formed via the injection of CO_2-rich fluids that caused the growth of coarse-grained secondary carbonate and calc-silicate minerals (fig. 4B; for example, Nutman and others, 1984; Rosing and others, 1996). However large pods in these ultramafic schist units are, in fact, massive and dominated by amphibole ± chlorite and devoid of obvious metasomatic effects such as carbonate and calc-silicate veins. At one locality near the western termination of the belt (65°06.891'N 50°12.681'W) possible relict pillow structure is present in a lacuna within these ultramafic schists. Two samples of homogeneous massive mafic schists (G93/23 and G05/07) from the western and eastern ends of the belt, respectively, have remarkably similar whole rock major and trace element compositions (table 1), indicating that they still preserve some original signatures of their igneous protoliths. These schists have high MgO (>25 wt%) and modest Al_2O_3 (>5 wt%; table 1), and plot on the high Al/Si side of primitive mantle compositions on the Mg/Si versus Al/Si diagram (fig. 5C). Based on these data, the rocks do not lie on the variably-depleted mantle trend, as found for ≥3800 Ma peridotites *ca.* 10 km south of the Isua supracrustal belt described by Friend and others (2002; fig. 5C). Instead they have higher Al/Si, typical of magmatic rocks derived from the mantle, such as Isua 3700 Ma picrite and 3800 Ma layered gabbros *ca.* 10 km south of Isua (fig. 5C; data from Friend and others, 2002; D'Andres and others, 2019).

One of the thin siliceous units within the Mafic Volcanic formation is exposed over >5 km west of lake 678 m (maps in Nutman and Friend, 2009). This siliceous unit is magnetite-bearing with low TiO_2 (0.01 wt%) and Al_2O_3 (0.24 wt%; Nutman and Friend, unpublished data) and is interpreted as originating from a siliceous banded iron formation protolith (see the Appendix for a summary of zircon geochronology on the sample G07/02 -04 from this unit, published in Nutman and others, 2009). At 65°05.28'N 50°10.75'W (fig. 3) this unit is intruded by a very fine-grained tonalite sheet (fig. 4C), resembling one <100 m to the north dated at 3803 ± 3 Ma by Crowley (2003). Therefore, these thin laterally continuous siliceous units are interpreted as sedimentary in origin with an age of >3803±3 Ma, and to represent breaks in basaltic volcanism when deep marine background sedimentation occurred. Alternatively, if they mark cryptic, layer-parallel tectonic breaks within the volcanic pile, then tectonism must have occurred at ≥3803 Ma, because the tonalite sheet at the G07/02, -04 locality is not sheared.

Mafic Volcanic Formation Upper Boundary and the Sedimentary Formation

Along much of its strike, the upper part of the Mafic Volcanic formation comprises the thickest unit of ultramafic schists with a likely picritic protolith. The upper boundary of this unit is marked by seams of siliceous and carbonate rich rocks. Some of the siliceous rocks are interpreted as quartz veins, which commonly bear fuchsite (Cr-bearing muscovite) with the chromium being derived from the adjacent ultramafic schists. Samples of likely vein origin, such as the one shown in figure 4E (65° 06.89'N 50°13.03'W), yielded no zircons. Mineral exploration companies have found sub-economic gold mineralization associated with the fuchsite-bearing veins. At other localities, thin (<2 m wide) discontinuous quartz-rich rocks such as G93/25 at the margin of underlying ultramafic schists (fig. 4B) have yielded oscillatory-zoned

zircons, with ages from 3890 to 3805 Ma and are interpreted as having sedimentary protoliths (Nutman and Collerson, 1991; Nutman and others, 2009). Detailed mapping throughout the ISB (condensed in fig. 3 and maps of the entire belt in Nutman and Friend, 2009) shows that this boundary, together with the seams of locally mineralized quartz veins and rarer detrital quartzite, truncates an ultramafic schist and amphibolite contact in the underlying unit. Given the presence of both detrital quartzites and tectonized, mineralized quartz veins at this contact, our preferred interpretation is that it was originally an angular unconformity, which has been tectonically modified, in many places to the extent of excision of lithologic units. The strong competency of the adjoining units would be a likely reason for strain partitioning along this boundary.

Also associated with the rare detrital quartzites at the base of the Sedimentary formation are discontinuous units of carbonate and carbonate + calc-silicate rocks whose thickness varies considerably along strike. In the cores of folds at the western termination of the belt outcrops are locally >100 m wide (fig. 3), whereas on fold limbs, they are reduced considerably in thickness, and may be entirely excized. The variable character of this unit is because its abundance in carbonate makes it extremely ductile and, combined with the presence of quartz, there is very widespread development of coarse-grained calc-silicate minerals, obliterating early textures.

The origin of these carbonate-rich rocks has been debated for several decades, with some workers suggesting *all* ISB carbonate-bearing lithologies are mafic and felsic silicate rocks that were strongly modified by Eoarchean carbonation (for example, Rosing and others, 1996; Myers, 2001). Others, whilst agreeing that metasomatism has left a substantial imprint on many ISB rocks, argue there are also present relicts of sedimentary carbonate rocks (Allaart, 1976; Nutman and others 1984, 2010, 2019). The latter authors point out that CO_2 metasomatism is a widespread feature of most metamorphosed and deformed volcanic and sedimentary rocks, and that the presence of metasomatic carbonate veins and calc-silicate mineralization does not preclude that sedimentary carbonate protoliths may also be present; all that metasomatic processes do is to make it more difficult to unravel the protoliths. A key problem caused by the superimposed amphibolite facies metamorphism is that if carbonate sedimentary rocks also contained silicate phases, then unless intergranular H_2O-rich fluid is excluded, the silicates and carbonates will react together to give calc-silicate minerals. If silicates and carbonate are present in the correct proportion, then at ≥500°C the influx of H_2O-rich fluid will result in massive amphibole rocks, which in the field superficially resemble altered mafic igneous rocks.

1974 to 1975 mapping by the late J. H. Allaart recognized elongate lenses of massive dolomite rock (fig. 4D) in the western part of the belt (65°05.46'N 50°07.04'W). These rocks occur in a <20 m broad belt of mixed calc-silicate and carbonate rocks between ultramafic schists to the north and the laterally-continuous felsic schist unit (Felsic Volcanic formation) to the south (fig. 3). Allaart's original dolomite rock sample (170728, table 1) has very low SiO_2 (3.19 wt%), Al_2O_3 (0.04 wt%), TiO_2 (0.02 wt %) with Rb/Sr <0.005 and a PAAS-normalized REE+Y trace element signature resembling that of seawater throughout Earth' s history (fig. 6A). This led Nutman and others (2010) to conclude this is a rare relict dolostone sedimentary rock. More trace element analyses from the dolomite rocks at this locality confirm the consistency of the REE+Y seawater-like trace element signature (fig. 6A). Additionally, the dolostone's $\delta^{13}C_{VPDB}$ is *ca.* +1‰, within the range of modern marine carbonate (table 2). This REE+Y signature is similar to that seen in Paleoarchean dolomitized stromatolites – rocks of unquestioned shallow marine origin (Van Kranendonk and others, 2003). On the other hand, a carbonate vein (sample G17/64) cutting Sedimentary

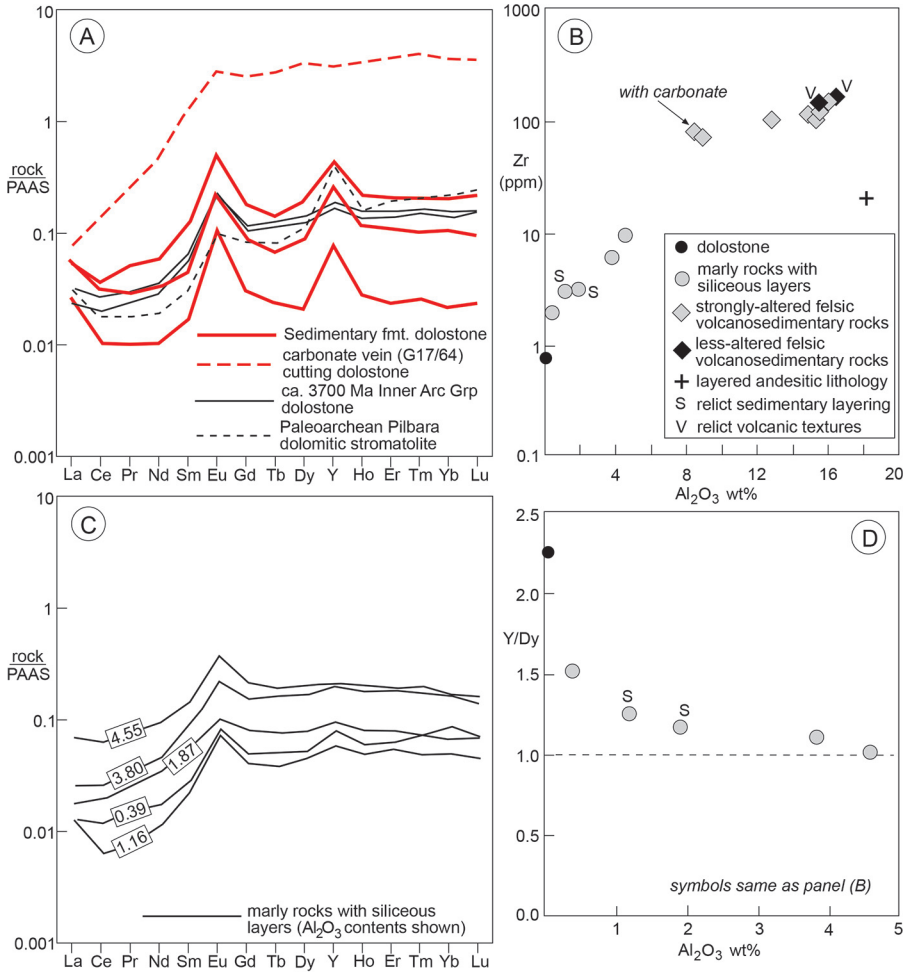

Fig. 6. Geochemistry of the Sedimentary formation. (A) PAAS-normalized REE+Y plot for 'pure' dolostone. Shown for comparison is a *ca.* 3700 Ma dolomitic stromatolite from the ISB Inner Arc Group (Nutman and others, 2016), a Paleoarchean Pilbara dolomitic stromatolite (Van Kranendonk and others, 2003) and a discordant carbonate vein in the Sedimentary formation. (B) Zr – Al_2O_3 plot. (C) PAAS-normalized REE+Y plot for Al-bearing dolomitic samples (some with relict sedimentary structures (fig. 4F). Numerals on lines are the Al_2O_3 (wt%) of the sample. (D) Y/Dy – Al_2O_3 plot (symbols the same as in panel B).

formation dolostone displays a completely different REE+Y signature, indicative that, by contrast, it is of intracrustal origin (fig. 6A).

Note in figure 4D that only 1 to 2 m away from the sampled pure dolostone, the unit has developed extensive growth of calc-silicate minerals (dol and c-s respectively in fig. 4D). This is because of the higher silica content in the protolith combined with the influx of H_2O-rich intergranular fluid during tectonothermal events. A thin metadiabase Ameralik dyke (*ca.* 3500 Ma) at this locality shows only minor carbonate reaction, indicating that most of the reaction between carbonates and silicates occurred in the Eoarchean.

In low-strain zones in fold hinges in the northwestern end of the ISB (fig. 3), transects through the carbonate-rich lithologies from ultramafic schists at the top of

the Mafic Volcanic formation towards the base of the Felsic Schist formation have an overall trend from massive very dolomite-rich to more layered, less-dolomitic lithologies, in which are some hitherto unrecognized low strain zones. In one fold core at 65°07'N 50°12.78'W delicate layering on a scale of a few centimetres or less is preserved over a few m^2 of outcrop (fig. 4F). This layering is graded, with sharp quartz-rich bases that grade up into a more dolomite-rich top. These rocks display quartz and dolomite largely in equilibrium, with only sparse reaction to give rise to calc-silicate minerals forming local selvedges. Farther west, near the margin of the ISB at 65° 07.13'N 50°13.07'W, similar layered rocks are preserved in another fold core, but there has been reaction between quartz and dolomite, giving rise to extensive growth of tremolite. Sample G17/62 from this second fold core yielded sparse small oscillatory-zoned zircons, with ages between *ca.* 3820 and 3805 Ma (see Appendix for details).

Geochemical analyses have been undertaken on a spectrum of these rocks, from the pure dolostones (sample 170728, fig. 6A) to increasingly layered and silicate-bearing ones (table 1). Using Al_2O_3 as indicator of silicate content, these rocks show a clear correlation with trace elements such as Zr (fig. 6B). Additionally, the corruption of the $REE+Y_{(PAAS\ normalized)}$ seawater-like signature recorded in the pure dolostones is linked with increase in Al_2O_3 (fig. 6C). This is also demonstrated by the $Y/Dy_{(PAAS\ normalized)}$ ratio from 2.6 in pure dolostone 170728 with Al_2O_3 of 0.04 wt%, reducing to unity in G17/47 with Al_2O_3 of 4.55 wt% (fig. 6D). Given that two of the analyzed samples (G17/52A, -B) have relict graded sedimentary layering (fig. 4F), we interpret these geochemical trends as sedimentary, with dolomite deposition being increasingly 'polluted' by an alumino-silicate component. This is supported by plots such as Zr versus Al_2O_3 (fig. 6B) showing the trend for the mixed sedimentary rocks is towards the field of volcanic Outer Arc Group rocks.

Felsic Volcanic Formation Field Characteristics

The Felsic Volcanic formation is in sharp contact with the underlying Sedimentary formation. The interpretation of the unit has been controversial due to the high strain and associated metamorphism, predominantly reducing the rocks to felsic schists. Because this formation forms the core of an early isoclinal fold (fig. 1), its top is not observed. This felsic schist unit is continuous for the length of the ISB for almost 30 km (fig. 1). Throughout the 1970s it was interpreted as an acid volcanic unit with large bombs preserved at one locality (Allaart, 1976). The unit was then investigated by Rosing and others (1996) who concluded that it represents a strongly metasomatized, carbonated tonalite sheet intruded into the belt, whilst Myers (2001) reinterpreted the felsic schists as a strongly metasomatized series of mafic volcanic rocks. Nutman and others (1984, 2015) agreed with an acid volcanic and/or volcanosedimentary origin, but proposed that the local 'bombs' are tectonic boudins formed out of more competent layers. Lines of evidence supporting a felsic protolith are the large yield of oscillatory-zoned igneous zircons from these rocks (Compston and others, 1986; Nutman and others, 2015) and, whilst overall strain is high, there is the local, rare preservation of graded layering, and survival of microtextures resembling fiammé (fig. 4a *in* Nutman and others, 1984) and vesicles (fig. 7C and Nutman and others, 2015) within the putative volcanic bombs. These latter authors also documented the deviation from igneous compositions, particularly high K_2O correlated with low Na_2O. Nutman and others (2015) also noted the high $\delta^{18}O_{VSMOW}$ of the whole rocks versus the 'normal' mantle-like values for igneous zircons in the same rocks (Hiess and others, 2009), which they interpreted as demonstrating near-surface alteration soon after deposition.

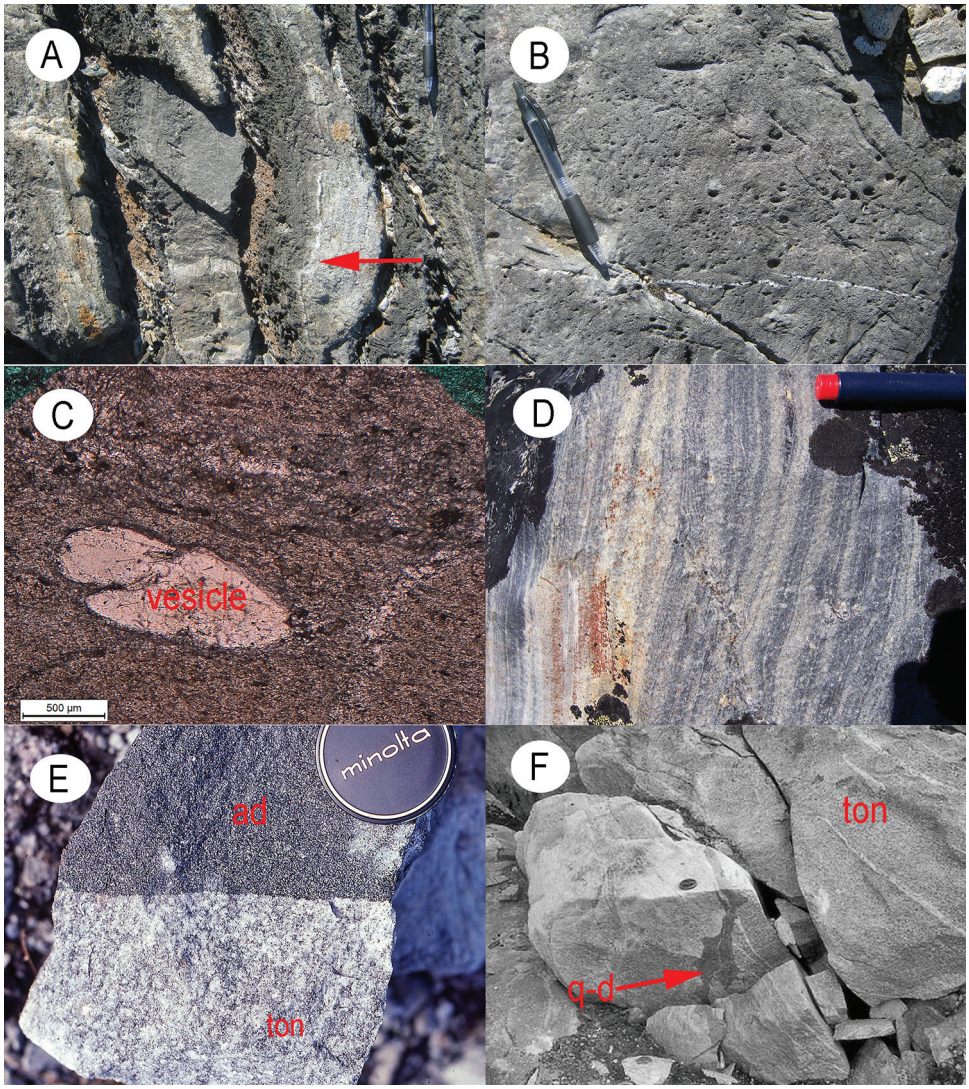

Fig. 7. Outcrop photographs of the Felsic Volcanic formation and the 3809-3803 Ma tonalites south of the Isua supracrustal belt. (A) Graded layering near base of the formation. There are repeated cycles of felsic schist units with a sharp base (right hand margins in the photograph), grading into calc-silicate-rich rock (product of metamorphic reaction between silicate minerals and dolomite, then into dolomite-rich rock. Proposed facing direction is shown by the red arrow. Pen for scale is 15 cm. (B) Massive felsic schist with relict vesicular texture (carbonate filled and then weathered-out on the surface) at the dating sample G17/59 locality. Pen for scale is 15 cm. (C) Photomicrograph of quartz-filled vesicle in felsic boudins within carbonate-rich layers (reproduced from Nutman and others, 2015). (D) Rare preservation of millimeter-scale lamination in the eastern exposures of the formation. Pen for scale is 15 cm. (E) Sampling locality of tonalite G97/18 (table 1 and analyses shown on fig. 8). The white speckled appearance is due to the presence of (recrystallized) plagioclase phenocrysts (note the positive Sr and Eu anomalies for this sample in Fig. 8C). Tonalite (ton) and *ca.* 3500 Ma Ameralik dyke (ad). Lens cap for scale is 5 cm diameter. (F) Flame-margined quartz diorite (q-d) coeval with *ca.* 3800 Ma tonalite (ton). Lens cap for scale in center of picture is 5 cm diameter.

Additionally, further low strain zones have been found in fold cores at the western end of the belt (fig. 3) that preserve relicts of other primary structures, which have not been reported previously. At 65°06.90'N 50°12.75'W, the margin of the Felsic Volcanic formation is separated from ultramafic schists to the west by a *ca.* 1 m thick

unit of calc-silicate rocks with relict carbonate (Sedimentary formation). The felsic schists display distinct compositional layering on a scale of 10 to 20 cm, whereby felsic schist grades into calc-silicate and then into dolomite-rich rock, with a sharp base with the next felsic schist layer (fig. 7A). The lithological cycle (from thin but massive quartzo-feldspathic rock to calc-silicate to carbonate) is repeated several times on this single outcrop. The inferred sense of the grading from felsic carbonate suggests younging *away* from the ultramafic schist outcropping to the west. The repeated asymmetry of these units is not compatible with metasomatic CO_2 introduction to give rise to the dolomite and calc-silicate. Instead we propose this is an original feature of the rock. Most likely is that between individual volcanic events there were interludes, during which the tops of volcanic layers were severely altered, plus carbonate was deposited.

At the center of a fold interference pattern (65°06.92'N 50°12.47'W; G17/59 locality), the Felsic Volcanic formation is dominated by massive felsic layers, some up to 10 m thick, separated by narrower zones with carbonate. Here, the massive felsic rocks are very fine-grained and consist of quartz + feldspar + muscovite. These have circular features of carbonate up to a few Millimeters across which weather-out on outcrop surfaces and are interpreted as vesicles (fig. 7B). We propose that these rocks formed as thick vesicular volcanic flows. Massive felsic schist sample G917/59 at this locality has small, oscillatory-zoned igneous zircons with a single weighted mean $^{207}Pb/^{206}Pb$ age of 3802±5 Ma (see Appendix).

Eastwards along the belt, the Felsic Volcanic formation becomes overall more finely-layered, with massive units much less common. The layering is more regular and continuous, with occasional thin interludes rich in carbonate and calc-silicate minerals. In rare domains of lesser strain, delicate sub-Millimeter-scale layering is preserved (fig. 7D). Therefore, following Nutman and others (2015), the layering in these rocks is regarded as volcano-sedimentary in origin, but in most places transposed by strong superimposed deformation.

Felsic Volcanic Formation and Coeval Tonalite's Geochemistry (3809–3803 Ma)

The most obvious non-magmatic feature in the major element chemistry of the Felsic Volcanic formation schists is the high K_2O (between 4 and 12 wt%) coupled with <1 wt% Na_2O (table 1; fig. 8A). The Rb-Sr variation in the felsic schists is also non-magmatic, with anomalously low Sr but similar Rb abundances compared to those in unaltered Eoarchean felsic plutonic rocks (fig. 8B and Nutman and others 2015). The REE and HFSE are generally thought to be resistant to post-magmatic alteration in igneous volcanic systems on which regional metamorphism has been superimposed (for example, Polat and Hofmann, 2003 and references therein). In a trace-element spider-plot (fig. 8C; normalized to primitive mantle values of McDonough and Sun, 1995), igneous features are strong negative Ti, Nb and Ta anomalies, as seen in plutonic tonalites to the south (demonstrated by sample G97/18 in fig. 8C). These features are likely to indicate supra-subduction magmatic systems, involving subcrustal retention of Ti, Nb and Ta during melt production (Nutman and others, 1999, 2015; Hoffmann and others, 2011b, 2019; Friend and Nutman, 2011).

The coarse-grained plutonic southern tonalites reported in Nutman and others (1999) are plagioclase phyric (fig. 7E) and generally have positive Sr and Eu anomalies (represented by sample G97/18 in fig. 8C). We contend that the 3808 to 3803 Ma southern tonalites and the igneous protoliths of the Outer Arc Group felsic schists are not only coeval but also consanguineous, such that the tonalites represent an intracrustal magma chamber, where crystallization and accumulation of phenocrystic plagioclase left the residual magma with negative Eu anomalies and overall higher total REE element content. Some of this residual magma was erupted, giving the

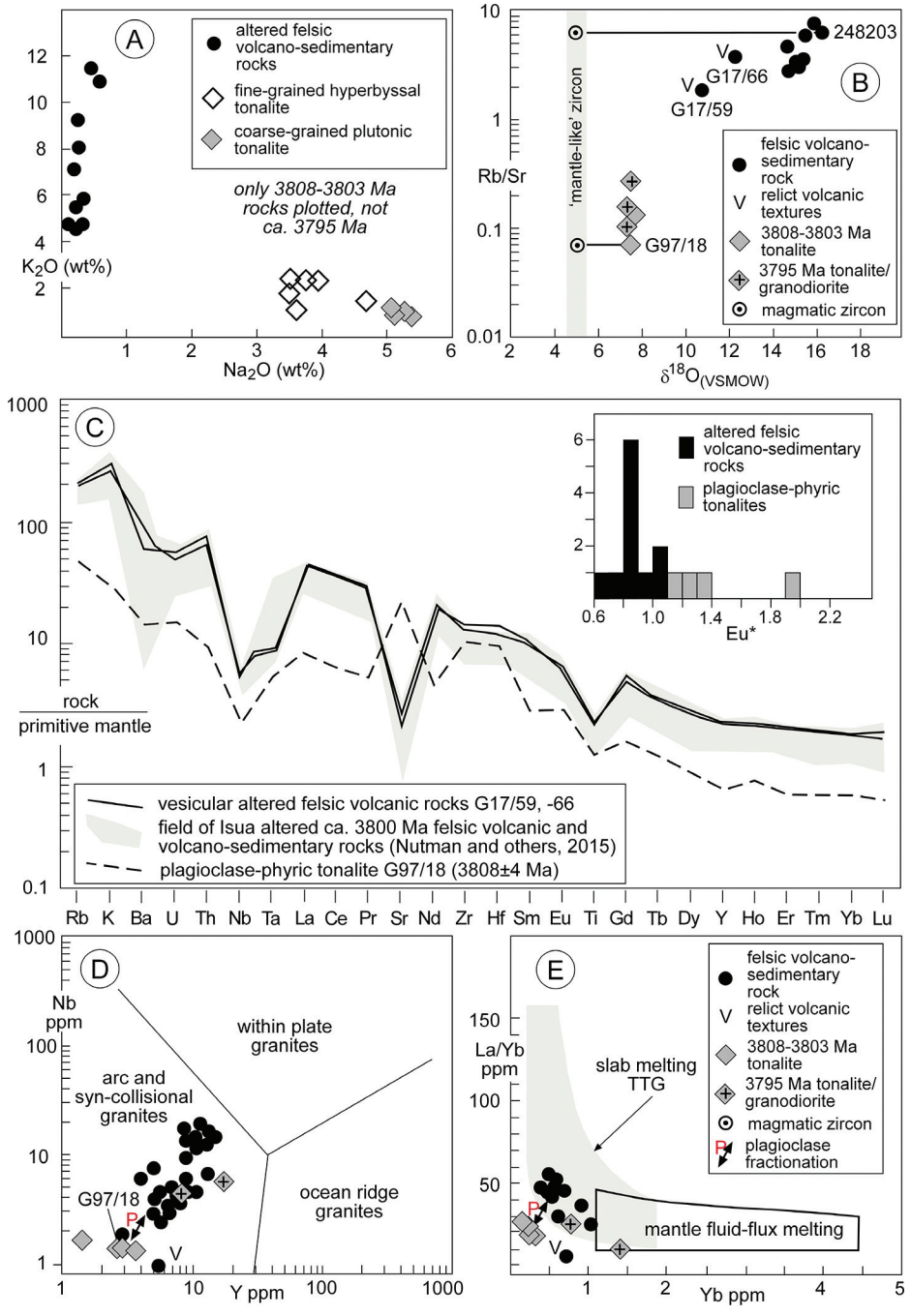

Fig. 8. Geochemistry of the Felsic Volcanic formation and coeval tonalites to the south. This uses analyses from Baadsgaard and others (1986b), Nutman and others (1999 and 2015), Hiess and others (2009) plus new data presented here. (A) K_2O –Na_2O (wt%) plot. (B) Rb/Sr – $\delta^{18}O_{VSMOW}$ (whole-rock) plot. (C) Primitive mantle normalized trace element plot (normalized with values of McDonough and Sun, 1995). (D) Nb-Y plot. (E) La/Yb-Yb plot (Martin, 1986).

TABLE 2

Oxygen isotope data

sample	type	$\delta^{18}O_{VSMOW}$ (‰)
Intrusive rocks		
G97/18[a]	tonalite	7.4
G97/18[b]	zircon	5.0
G93/44[a]	tonalite	7.6
292128[a]	quartz diorite	6.6
225858[c]	tonalite	6.5
225943[c]	tonalite	7.3
225841[c]	tonalite	7.3
225909[c]	tonalite	7.5
225943[c]	tonalite	7.3
225942[c]	tonalite	7.5
225841[c]	tonalite	7.3
Felsic Volcanic formation		
G93/24[a]	felsic schist	14.7
G04/68[a]	felsic schist	15.1
G04/69[a]	felsic schist	14.6
G11/76[a]	felsic schist	15.8
G11/77[a]	felsic schist	15.4
G11/78[a]	felsic schist	15.3
G11/79[a]	felsic schist	15.0
248203[a]	felsic schist	16.2
G17/59[c]	felsic schist	10.7
G17/66[c]	felsic schist	12.2
248202[b]	zircon	5.0
248203[b]	zircon	4.9
Mafic Volcanic formation		
14-07[d]	basalt	6.3
15-07[d]	basalt	6.8
16-07[d]	basalt	5.1

Sources: a. UOW stable isotope laboratory; b. Hiess and others (2009); c. Baadsgaard and others (1986b); d. Pope and others (2012).

geochemical signature seen in the felsic schists of the Felsic Volcanic formation (fig. 8C). The Nd and Hf isotopic signatures support this genetic linkage between the 3808 to 3803 southern tonalites and the Outer Arc Group felsic schist unit, because they have the same juvenile crustal ^{176}Hf and ^{143}Nd initial isotopic signatures (data compiled from Jacobsen and Dymek, 1988; Bennett and others, 2007; Hiess and others, 2009).

On the other hand, the southern tonalites and the Felsic Volcanic formation felsic schists display different oxygen isotopic signatures (fig. 8B). The magmatic zircons in felsic schist sample 248203 and representative southern tonalite sample G97/18 have the same $\delta^{18}O_{VSMOW}$ values of *ca.* +5‰ (Hiess and others, 2009). In contrast, the whole rocks from which the zircons were derived show different oxygen isotope signatures (Nutman and others 2015 and table 2), with the $\delta^{18}O_{VSMOW}$ of the tonalites at +7 to +8‰ versus the felsic schists at +10 to +16‰ (fig. 8B). In the felsic schists, less-altered massive vesicular samples G17/59 and −66 have both the lowest $\delta^{18}O_{VSMOW}$ and Rb/Sr values. This supports the conclusion of Nutman and others (2015) that the felsic schists are volcanic rocks that experienced strong alteration in a low temperature environment, with the shift in Rb/Sr caused by the breakdown of plagioclase, releasing Sr. This process would not be expected to fractionate Eu versus Gd and Sm, but would lead to significant reduction of Sr versus Nd and Pr. This is shown

in figure 8C, where the size of the Sr negative anomaly is much more pronounced than the Eu negative anomaly (Eu*/Sr* is 7 to 26; where Sr*=Sr/(Pr+Nd)*0.5 and Eu*=Eu/(Sm+Gd)*0.5). As concluded by Nutman and others (2015), the more marked depletion of Sr could be related to low temperature breakdown of plagioclase, with Sr (and Na) removal in solution. A similar signature is seen in other early Archean volcanic rocks, such as *ca.* 3460 Ma Kittys Gap rocks of the Warrawoona Group, Pilbara craton (Smithies and others, 2007).

DISCUSSION

U-Pb Zircon Geochronology of the Outer Arc Group and Tonalite-dominated Terrane to the South

This geochronological appraisal is based on new data from samples G17/59 and G17/62 combined with previous results by the authors of this paper (see Nutman and Friend, 2009) plus one age determination by Compston and others (1986) and several by Crowley (2003). For the new data, see Nutman and others (2019) for the analytical, data reduction and assessment methods and Appendix 1 for the data and detailed interpretation.

The Mafic Volcanic formation amphibolites and associated meta-picrites are devoid of protolith zircon, but their age is constrained to ≥3803±3 Ma via a tonalite sheet that cuts them (figs. 2 and 3; Crowley, 2003). In the southern tonalite area, a similar age constraint is derived for amphibolite enclaves (with both volcanic and gabbro protoliths), because they are cut and enveloped by tonalites with ages of up to 3809±4 Ma (Friend and others, 2002).

At the base of the Sedimentary formation are found vestiges of a sedimentary quartzite unit, which contains detrital zircons ranging in age from 3890 to 3805 Ma (fig. 2). Of note is the preponderance of *ca.* 3850 Ma zircons in these quartzites (data compiled by Nutman and others, 2009). 3850 Ma does not match ages of rocks in the tonalite-dominated terrane for >15 km south of the ISB, but rare tonalites of that age are found scattered in the southern part of the Itsaq Gneiss Complex, up to 150 km away (Nutman and others, 2007b). Thus, the provenance of the quartzites is mixed, with detrital components having an age span of *ca.* 80 million years.

Detailed mapping of the fold interference pattern in the western end of the belt which was compiled into the small-scale map shown in figure 3, combined with whole rock geochemistry (fig. 6), suggests the amount of felsic material in these sedimentary rocks increases in the direction of inferred younging. These rocks give a low yield of detrital zircons, as demonstrated by sample G17/62 (detailed discussion in Appendix), which displays a much narrower age range of *ca.* 3820 to 3805 Ma than the quartzites lower down in the formation. The ages of these grains are congruent with that of the tonalites south of the ISB (Nutman and others, 1999; Crowley, 2003) and, except for the few *ca.* 3820 Ma grains, are congruent with the volcanic protolith ages for the Felsic Volcanic formation. The felsic schists derived from volcanic and volcano-sedimentary rocks in the overlying Felsic Volcanic formation all have unimodal zircon populations ranging in age from 3802±4 to 3807 ±6 Ma. Combining these individual age determinations into a single weighted mean calculation yields an age of 3806±3 Ma (95% confidence, MSWD=0.27). Thus, it is probable that the felsic volcanism lasted less than 6 million years.

Integrated Evolution of the Outer Arc Group and Tonalite-dominated Terrane to the South

Combined field observations and mapping, with geochemistry and geochronology, provide a detailed evolutionary history for the Outer Arc Group and the tonalite-

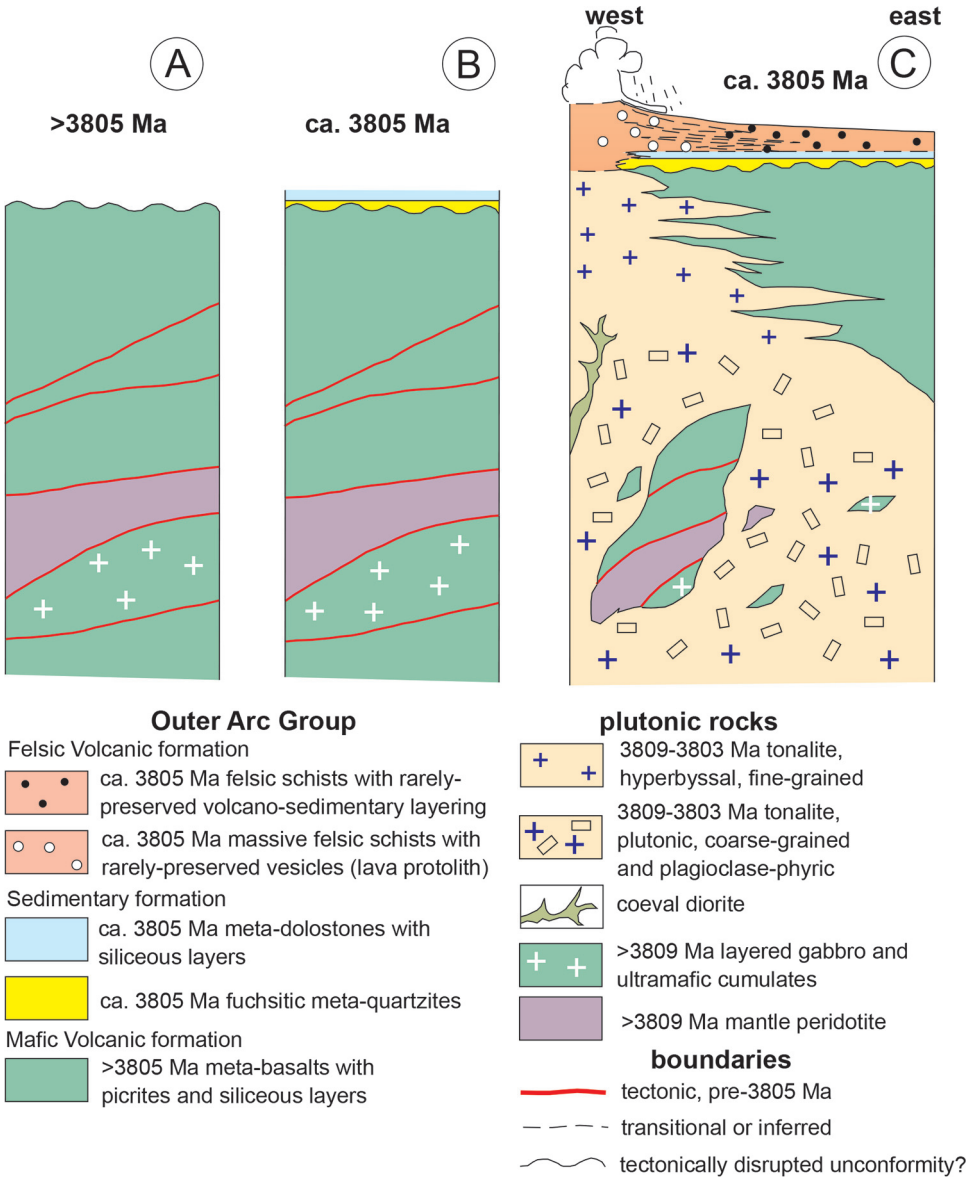

Fig. 9. Time sequence cartoon showing evolution of the Outer Arc Group and the tonalite-dominated terrane to the south, from >3809 Ma to *ca.* 3805 Ma. See text for explanation.

dominated terrane to the south that lasted for a short time around 3800 Ma. The Outer Arc Group Mafic Volcanic formation and the amphibolite, ultramafic and rare sedimentary enclaves in the southern tonalites have not been dated directly, but they must be >3800 Ma based on ages of the intrusive tonalite sheets. In the southern tonalites, detailed mapping reveals that amphibolites of both volcanic and gabbroic protoliths were intercalated with depleted mantle abyssal peridotite lenses before the tonalites were intruded, pointing to an important tectonic event at ≥3809±4 Ma (fig. 9A; Friend and others, 2002). We propose that this tectonic intercalation of upper

mantle (Friend and others, 2002) and crustal rocks resulted in crustal thickening and is possibly reflected by the proposed angular unconformity (later tectonically modified) at the top of the Mafic Volcanic formation (fig. 9A).

Deposition of the Sedimentary formation started with the rare fuchsite quartzites, in which the youngest detrital zircons are 3805 to 3810 Ma, giving the maximum time of deposition (fig. 9B). 'Pure' dolostones in this sedimentary unit have a seawater-like REE+Y signature (fig. 6A), which from the detailed analysis of ancient chemical sedimentary rocks by Kamber and others (2014) indicates deposition was most likely in an open marine environment, rather than an enclosed basin. Upper parts of the sedimentary unit show influx of a felsic component into the deposition of dolomite and silica, with rare detrital zircons matching the age of overlying felsic volcanic rocks and the coeval southern tonalites. Furthermore, at rare low strain localities in the likely base of the Felsic Volcanic formation, there is graded interlayering between the felsic schists and dolomitic rocks (fig. 7A). We propose that the deposition of *ca.* 3805 Ma dolostones and interlayered siliceous rocks was progressively swamped by increasing felsic volcanism, and as such in figure 2 and figure 9 this boundary is shown as transitional.

We propose that the southern tonalites represent the magma chamber that fed the felsic volcanism of the Felsic Volcanic formation. The cooling magma in the chamber was crystallizing plagioclase phenocrysts (shown schematically in the lower part of fig. 9C), whose accumulation gave the positive Eu and Sr anomalies of tonalites such as sample G97/18. Batches of the residual tonalitic magma erupted as the volcanic protoliths of the felsic schists, which show the expected muted negative Eu anomalies. There are volumetrically minor quartz diorites associated with the tonalites, as demonstrated not only by zircon U-Pb geochronology (for example, sample 292128; table 1), but also by the flamed-margins of small quartz diorite sheets in the tonalites, indicating coexisting magmas of different composition (fig. 7F). The volcanic equivalents are probably rare andesitic bodies within the Felsic Volcanic formation. The felsic volcanic rocks underwent severe near surface alteration or weathering. This gave rise to their elevated $\delta^{18}O_{VSMOW}$ values, almost complete loss of Na and gain in K, attributed to breakdown of plagioclase (Nutman and others, 2015), which can explain the amplification of the negative Sr anomaly over the Eu anomaly.

The mapping of the Felsic Volcanic formation indicates that more massive lithologies occur in the west, including units up to several metres thick in which vesicular texture is preserved (fig. 7B). Eastwards, the schists become overall more closely layered, and in rare low strain zones, very fine-scale lamination is preserved (fig. 7D). Therefore, we interpret that the rocks at the western end of the belt were originally more proximal to the feeder vent(s). At the western termination of the ISB, the amphibolites of the Mafic Volcanic formation are truncated by intrusions of very fine-grained tonalite and quartz diorite, in proximity to the overlying felsic volcanic rocks (fig. 3). These field relationships are consistent with this being the feeder stock, but more work is needed on this poorly exposed part of the belt to confirm this (figs. 2, 3 and 9).

The final event in the *ca.* 3800 Ma crustal evolution was the intrusion of *ca.* 3795 Ma tonalite/granodiorite along the southern margin of the Inner Arc Group (figs. 1, 2, 3 and 9). Besides the age difference, the *ca.* 3795 Ma intrusions are more potassic than the *ca.* 3805 Ma tonalites, and at the margin of the belt they are distinctly more coarse-grained than the very fine-grained tonalite sheets dated at 3803±3 Ma by Crowley (2003).

Geochemistry and Geodynamic Setting of the Outer Arc Group and Tonalite-dominated Terrane to the South

The >3803 Ma Mafic Volcanic formation amphibolites derived largely from pillow basalts, display enrichment of the LREE over the HREE and negative Nb, Ta and

Ti anomalies (fig. 5A; Polat and Hofmann, 2003; Jenner and others, 2008; Hoffmann and others, 2011a). On the Th/Yb versus Nb/Yb discriminant plot (fig. 5B) the amphibolites lie in the arc field, for magmas generated by the fluid fluxing of peridotite by subduction-related fluids. Thus, their compositions are neither in the N-MORB–E-MORB mantle decompression melting array, nor do they match in composition komatiite and komatiitic-basalt compositions, as shown by the data compiled from Sossi and others (2016; fig. 5B). Thus, we concur with Polat and Hofmann (2003), Jenner and others (2009) and Hoffmann and others (2011a) that these rocks have geochemical signatures resembling Phanerozoic arc-related basalts. Oxygen isotope data on these amphibolites extracted from the literature (Pope and others, 2012) shows whole rock $\delta^{18}O_{VSMOW}$ mostly between +5 and +7 ‰, demonstrating no significant deviation from values expected for basaltic igneous protoliths. This would indicate there was only limited seafloor alteration of these basalts when erupted.

The Felsic Volcanic formation schists and the coeval southern tonalite samples share the same negative Nb, Ta and Ti anomalies in primitive-mantle-normalized plots (fig. 8C). Using Nb and Y (fig. 8D), elements likely to have been least modified by post-igneous processes, the southern tonalites and the felsic schist samples plot well within the volcanic arc granites field of Pearce and others (1984), and the eclogite-melting field of Archean tonalites in the La/Yb versus Yb diagram of Martin (1994; fig. 8E). Therefore, the igneous protoliths of both the tonalites and the felsic schists are regarded to have formed from arc-related, evolved, siliceous magmas.

Comparison of the Inner and Outer Arc Groups

Dominant lithologies within the ~3700 Ma assemblage of the Inner Arc Group are amphibolites and schists derived from basaltic, picritic, boninitic and andesitic volcanic rocks, felsic volcanic rocks, felsic volcano-sedimentary, and chemical sedimentary rocks, particularly chert and BIF, plus dolomitic rocks also of sedimentary origin (for example, Allaart, 1976; Nutman and others, 1984, 2007, 2009, 2010, 2013, 2016; Dymek and Klien, 1988; Komiya and others, 1999; Polat and others, 2002; Polat and Hofmann 2003, Bolhar and others, 2004, 2005; Furnes and others, 2007). Gabbros and ultramafic rocks are volumetrically minor compared to sedimentary and volcanic rocks (for example, Dymek and others, 1988; Friend and Nutman, 2011). In both the Inner and Outer Arc Groups basalts and picrites erupted in submarine environments are the oldest lithologies, and were followed by a transition to more silica-rich volcanic rocks. In both groups, early volcanic packages are succeeded by chemical sedimentary rocks. In the northeast of the ISB, there is a locally-preserved unconformity, albeit in most places this relationship has been obliterated by Eoarchean tectonothermal events (Nutman and Friend, 2009; Nutman and others, 2019). In the Outer Arc Group an unconformity is inferred between the top of the Mafic Volcanic formation of pillow basalts and the Sedimentary formation sedimentary rocks (fig. 2).

Eoarchean Geodynamic Regime of the Isua Area

More than fifty years ago, similarities between the ISB rocks and ophiolitic assemblages were documented by Keto and Kurki (1967). The reason for this was the ISB's lithological association resembling the 'Steinman trinity' (Steinman, 1905) of (meta) basalts, peridotite and chemical sedimentary rocks. In the following decades this view has been modified into a suprasubduction zone setting, with most rocks interpreted as having formed in arc-like environments (for example, Polat and Hofmann, 2003; Dilek and Polat, 2008). Where best preserved in the ISB, *ca.* 3700 Ma Inner Arc Group intercalated lithologies are boninite-like volcanic rocks,

basalts, andesites, andesitic volcano-sedimentary rocks, dacites and mantle metaserpentinite with the latter exhumed from depths where the confining pressure was >2Gpa (Polat and others, 2002, 2003; Appel and others, 2009; Friend and Nutman, 2010, 2011; Nutman and others, 2020). The boninitic rocks, basalts and andesites have geochemical features indicating melt production by fluid-fluxing of peridotite, *not* (nominally anhydrous) decompression melting (Polat and others, 2002, Polat and Hofmann, 2003). This association, particularly with the presence of boninite-like pillow lavas and exhumed high-Mg serpentinite, strongly resembles sediment-starved Phanerozoic arc-forearc sequences, as summarized by Stern and others (2012).

Because they considered that the models for Isua were based on an idiosyncratic interpretation of the field geology and geochronology, Webb and others (2020) have suggested a radical re-interpretation of the Isua area' geology; that the 3800 and 3700 Ma crust formed vertically in a stagnant lid/heat pipe regime, followed by a single metamorphic and structural event (Webb and others, 2020, their fig. 5D and 5E). Here, we outline four key points where observations on the rocks and their geochemistry conflict with the Webb and others' interpretation.

1. A major geological problem with Webb and others' concept of forming the ISB vertically in a stagnant lid is that *ca.* 3700 Ma mafic (≥1000°C) and TTG (≥800°C) magmas must have ascended through the *ca.* 3800 Ma package (both the Outer Arc Group and the extensive southern *ca.* 3800 Ma TTG). However, nowhere in the ISB do the *ca.* 3800 Ma Outer Arc Group rocks have intrusions of either Eoarchean mafic dikes or TTG rocks dated at 3700 Ma.
2. The mafic rock geochemical signatures all point to suprasubduction zone scenarios for juvenile crustal genesis, via fluid-fluxing of mantle peridotite, with even boninite-like rocks being significant (for example, Polat and others, 2002; Polat and Hofmann, 2003; Jenner and others, 2009 and onwards). In connection with the geochemical signatures for mafic rocks, it is noteworthy that no researchers have found Eoarchean mafic volcanic rocks in the ISB with the geochemical signatures of komatiites, komatiitic basalts or MORB-like rocks – whose genesis is by 'dry' adiabatic decompressional melting. Such magma genesis is the essential element in 'vertical' crust formation scenarios such as exemplified by the Paleoarchean of eastern Pilbara (Western Australia), yet it is absent from the ISB. This is demonstrated here by a Th/Yb – Nb/Yb plot (fig. 5B) comparing Outer Arc Group Mafic Volcanic formation rocks with average MORB, E-MORB and komatiite samples from Sossi and others (2016).
3. Webb and others (2020) also propose that there is just one homogeneous metamorphic event across the belt. This ignores the published data indicating that within the ISB there are panels of rocks with quite different Eoarchean peak conditions and at different times. These range from the kyanite-staurolite-garnet, Barrovian-style metamorphism found in metasedimentary rocks in the northeast (Boak and Dymek, 1982; Rollinson, 2002; Gauthiez-Putallaz and others, 2020) to the co-existence of olivine and titanian humite group minerals that indicate exhumation from the mantle (Friend and Nutman 2011; Guotana and others, 2019; Nutman and others, 2020). The Eoarchean juxtaposition of these metamorphic assemblages with other units displaying higher T/P amphibolite facies conditions is not explained by the vertical crustal evolution model.
4. The present arcuate geometry of the ISB is *not* the result of a single event, as demonstrated by multiple previous publications (for example, Nutman and

others, 2002), and not due to vertical tectonics as would be expected in a heat-pipe tectonic regime (for example, Collins and others, 1998). There was already a complex structural evolution before the Paleoarchean (*ca.* 3500 Ma) Ameralik dykes were intruded (Nutman 1986), upon which was superimposed a regional Neoarchean fold (coeval with amphibolite facies metamorphism). This is demonstrated by the arcuate open folding of the Paleoarchean Ameralik dykes and development of amphibolite facies assemblages within them.

On this basis, we contend that a suprasubduction zone/arc followed by orogenic crustal thickening interpretations are still the most viable options to explain the Eoarchean crustal evolution of the entire Isua area.

CONCLUSIONS

1. Despite subsequent repeated tectonic disruption and metamorphism episodically throughout the Archean, the Outer Arc Group of the Isua supracrustal belt has a recognizable lithological sequence and is divided into three formations.
2. The oldest part of the Outer Arc Group is the Mafic Volcanic formation dominated by submarine basalts with arc-like geochemical signature, lesser picrite and with some chemical sedimentary horizons. This formation's age is definitely $> 3803 \pm 3$ Ma, but probably $\geq 3809 \pm 3$ Ma. The mafic volcanic rocks have geochemical signatures of a supra-subduction zone arc setting.
3. The top of the Mafic Volcanic formation is interpreted as an unconformity upon which there are vestiges of a sedimentary detrital quartzite layer, strongly modified by tectonism.
4. The overlying Sedimentary formation has scattered occurrences of tectonized clastic quartzites at its base, where the youngest of its *ca.* 3805 to 3890 Ma detrital zircons provide the *maximum* age of deposition. 'Pure' dolostones with seawater-like REE+Y trace element patterns in this formation transition into carbonate-rich rocks 'polluted' by a felsic (volcanic?) component.
5. Uppermost is the Felsic Volcanic formation of 3807 to 3802 Ma felsic and intermediate volcanic rocks, which upon eruption were severely altered in a surficial environment. Coeval tonalites south of the ISB represent the intracrustal magma chambers that fed the volcanism.
6. The ISB's Inner and Outer Arc Groups are products of convergent plate boundary processes within a mobile lid geodynamic regime, *not* of a non-uniformitarian stagnant lid regime postulated by some researchers.

ACKNOWLEDGMENTS

Current work on the Isua supracrustal belt is supported by Australian Research Council Discovery Grants DP170100715 and DP180100103. Shane Paxton is thanked for zircon separations from samples G17/59 and G17/62, and we thank him for all the challenging mineral separations that he undertook for us over 2 decades. We also thank Guest Editor Simon Wilde and reviewer Stephen J. Mojzsis for their helpful comments.

APPENDIX

ADDITIONAL U-Pb ZIRCON GEOCHRONOLOGY

See Nutman and others (2019) for summary of analytical method, data reduction protocol and assessment. Sample G17/62 (fig. A1; 65°07.127'N 50°13.072'W and 3 ppm Zr) is a layered metasedimentary rock with a dolomitic siliceous marly protolith. It shows growth of tremolite, unlike the best-preserved dolomite + quartz and tremolite-free examples described above. The more altered sample was chosen for geochronology, so as not to sacrifice for zircon separation >1 kg of the best rare samples. The sample gave a yield of <30 zircons. Several grains appear dull or patchy in cathodoluminescence (CL) imaging. Analyses on such grains registered high ^{204}Pb count rates showing disturbance, and hence these analyses were aborted. Twenty-three analyses were completed on 21 grains (table A1). These gains are small (<100 μm) euhedral to subhedral prisms with variably-preserved fine-scale oscillatory zoning parallel to the grain exteriors. ~50 μm grain fragment #15 is dull in CL imaging and has a Th/U ratio of 0.012. ~100 μm grain #20 has a core of oscillatory-zoned zircon and an overgrowth dull in CL imaging and a Th/U ratio of 0.005. Both of these low Th/U analyses yield concordant Neoarchean ages, with a weighted mean ^{207}Pb/^{206}Pb age of 2622±17 Ma (MSWD=0.32). They are interpreted as metamorphic in origin. Metamorphic zircon is very rare in Isua supracrustal belt rocks. We propose that metamorphic zircon growth in this sample is due to its proximity to the western margin of the belt, which is truncated by post-Paleoarchean shear zones. Continuation of these shear zones *ca.* 15 km to the south (at 65°01.25'N 50°18'74W) contain syn-kinematic pegmatites, which have a similar Neoarchean age of *ca.* 2635 Ma (Nutman, unpublished data). The variably-recrystallized oscillatory-zoned zircons have much higher Th/U (typically >0.5) and yield ^{207}Pb/^{206}Pb ages ranging from *ca.* 3710 to 3820 Ma. Those with the apparently youngest ages are most discordant (fig. A1) and are regarded to have undergone ancient loss of radiogenic Pb. This is supported by duplicate analyses on two grains. Grain #10 yielded ^{207}Pb/^{206}Pb ages of 3713 and 3805 Ma, whereas grain #6 yielded indistinguishable duplicate ^{207}Pb/^{206}Pb ages of 3808 Ma. Based on the analyses with close to concordant U-Pb ages, the youngest grains with most reliable ages are thus 3808 to 3803 Ma. Binned as a histogram, ≥3803 ages do not show a unimodal distribution (table A1, fig. A1). The problem with assessing these analyses is that any difference in age is small relative to analytical error, and that only 21 small grains are suitable for analysis. Using the simplest statistically valid interpretation, they are all indistinguishable within analytical error, with a weighted mean ^{207}Pb/^{206}Pb age of 3811±4 Ma (MSWD=0.42). However, if the granularity of the data suggested by the binned data is authentic, three age components could be present; 3807±6 Ma (MSWD=0.11), 3812±8 Ma (MSWD=0.01) and 3819±9 Ma (MSWD=0.03). Given the reproduction of a 3808 Ma age from two analyses on grain #6, this second interpretation is preferred. In which case, the *maximum* time of deposition is placed at 3808 to 3803 Ma and the sample contains some slightly older grains, which match in age some tonalites south of the ISB (Nutman and others, 1999).

Sample G17/59 (fig. 3; 65°06.967'N 50°12.233'W and 140 ppm Zr) is from a low strain zone in a Felsic Volcanic formation massive unit with relict vesicles (fig. 7B). The sample gave a high yield of small (<150 μm) euhedral to subhedral prismatic zircons. CL images display variably-recrystallized fine-scale oscillatory zoning parallel to the grain exteriors. Sixteen analyses were undertaken on 15 grains. All analyses have high Th/U ratios (1.1 to 0.4) typical of magmatic zircon and all have close to concordant ages (table A1, fig. A1). With the exclusion of analysis #5.1 with the lowest apparent ^{207}Pb/^{206}Pb age, the remainder yielded a weighted mean ^{207}Pb/^{206}Pb age of 3802±5 Ma (MSWD=0.36). This is interpreted as the eruption age of the sample's volcanic protolith.

Samples G07/02 and -04 of the siliceous banded iron formation in the Mafic Volcanic formation yielded <20 zircons (Nutman and others, 2009), with most being 150 to 100 μm long, which is unusually large for detrital zircons extracted from banded iron formation. Most grains have slightly discordant U-Pb ages with Eoarchean $^{207}Pb/^{206}Pb$ ages of <3800 Ma, that is, younger than the likely age of the intrusive tonalitic sheet. The smallest zircon yielded a $^{207}Pb/^{206}Pb$ age of 3898 Ma and is considered a genuine rare detrital grain. The <3800 Ma larger grains generally have higher U-content and less well-preserved oscillatory zoning (fig. 10 in Nutman and others, 2009). These could be either disturbed >3800 Ma grains or could be laboratory contaminants, because Eoarchean orthogneisses rich in zircon were processed in the same batch.

Petrographic Descriptions

Dolostones, sedimentary formation.—Two samples G12/84 and G17/40 show different characteristics. Both samples have a granoblastic texture and consist of >95% dolomite, but in G17/40 quartz and dolomite are mostly in equilibrium, with localized thin development of calc-silicate at mutual grain boundaries, but in G12/84 there is no quartz, and dolomite is in equilibrium with diopside and tremolite (fig. A2). The $\delta^{13}C_{VPDB}$ of G12/84 is +0.86‰. Because CO_2-liberating calc-silicate forming reactions reduce the $\delta^{13}C$ of the residual carbonate, the $\delta^{13}C$ value in the sedimentary protolith would have been slightly higher. Minor accessory minerals in the dolostones are tiny (<20 μm) sulfide grains.

Layered quartz- and dolomite-rich rocks, sedimentary formation.—Sample G17/44B is from the same outcrop as G17/52A,B for which we report geochemical analyses in this paper. Sample G17/44B consists of predominantly fine-grained quartz with lesser carbonate with a granoblastic texture and scattered biotite flakes (fig. A3). On the scale of the thin section, there is variation in the amount of carbonate, giving a compositional layering. Equilibrium contacts between quartz and dolomite are observed between many grains, but there is patchy development of tremolite between them. Small disseminated opaque grains (sulfide?) are the commonest accessory mineral, and very rare small zircons are observed.

Massive felsic unit, felsic volcanic formation.—Several samples are from the same outcrop of massive felsic rocks (G17/59 (used for zircon geochronology), G17/65 and -66). They have a very fine-grained matrix of quartz + feldspar + biotite + muscovite ± carbonate, with the scattered micas forming a weak foliation (fig. A4). There are sparse rounded quartz grains, which are interpreted as deformed corroded phenocrysts (fig. A4). Also present are scattered rectangular aggregates of muscovite + epidote ± quartz ± carbonate (fig. A5). These we interpret as pseudomorphs after sparse euhedral plagioclase phenocrysts. Rarer are grains of amphibole exhibiting brown pleochroism with green hornblende rims (fig. A6). These we interpret as rare, partly recrystallized, kaersutite phenocrysts. In the illustrated example the phenocryst is within a domain with a larger grain size (demarcated by red lines) than the typical matrix. In this case, the phenocryst could be within a small clast of slightly coarser-grained rock.

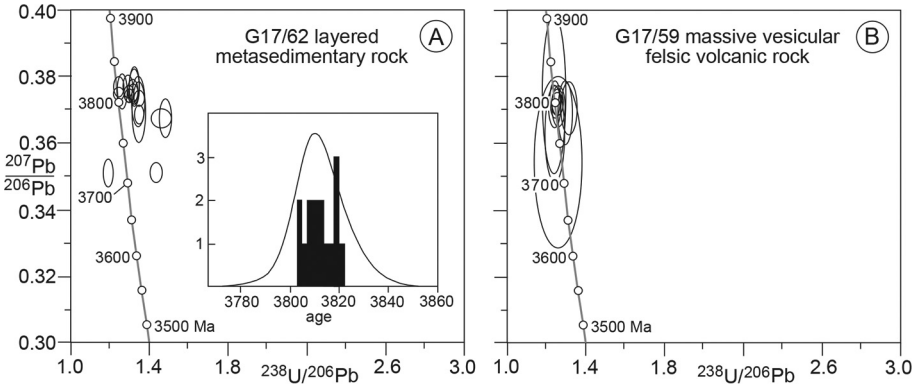

Fig. A1. Summary U-Pb zircon geochronology for new results from the Outer Arc Group. (A) $^{207}Pb/^{206}Pb$ - $^{238}U/^{206}Pb$ concordia diagram for layered metasedimentary rock G17/62 of the Sedimentary formation. The inset is a histogram and cumulative frequency distribution diagram for the analyses. (B) $^{207}Pb/^{206}Pb$ - $^{238}U/^{206}Pb$ concordia diagram for massive felsic schist G17/59 of the Felsic Volcanic formation, interpreted as a vesicular felsic volcanic rock.

TABLE A1

Zircon U-Pb data

labels	site	U ppm	Th ppm	Th/U	comm 206%	$^{238}U/^{206}Pb$ ratio	$^{207}Pb/^{206}Pb$ ratio	$^{207}Pb/^{206}Pb$ date (Ma)	%conc
G17/62 layered sedimentary rock, Sedimentary formation									
1.1	e,osc,p	81	43	0.53	0.14	1.287 ± 0.016	0.3769 ± 0.0023	3819 ± 9	97
2.1	e,osc,p	127	52	0.41	0.04	1.293 ± 0.015	0.3747 ± 0.0018	3811 ± 7	97
3.1	m,osc,p	356	189	0.53	0.03	1.237 ± 0.015	0.3751 ± 0.0016	3812 ± 6	100
4.1	e,osc,p	98	59	0.60	0.09	1.311 ± 0.016	0.3757 ± 0.0021	3815 ± 9	96
5.1	e,osc,p	139	70	0.50	0.05	1.273 ± 0.015	0.3732 ± 0.0020	3804 ± 8	98
6.1	e,osc,p	409	255	0.62	0.19	1.291 ± 0.015	0.3741 ± 0.0013	3808 ± 5	97
6.2	e,osc,p	452	270	0.60	0.07	1.245 ± 0.014	0.3741 ± 0.0016	3808 ± 6	100
7.1	m,osc,p	110	42	0.38	0.05	1.258 ± 0.016	0.3754 ± 0.0035	3813 ± 14	99
8.1	m,osc,p	153	90	0.59	0.36	1.431 ± 0.017	0.3513 ± 0.0019	3713 ± 8	92
9.1	e,osc,p	336	201	0.60	0.07	1.455 ± 0.033	0.3673 ± 0.0019	3781 ± 8	89
10.1	m,osc,p	438	185	0.42	0.06	1.346 ± 0.015	0.3734 ± 0.0015	3805 ± 6	94
10.2	e.osc,p	85	44	0.52	0.17	1.344 ± 0.018	0.3659 ± 0.0037	3775 ± 15	95
11.1	m,h,p	194	57	0.30	<0.01	1.186 ± 0.014	0.3513 ± 0.0027	3713 ± 12	106
12.1	m,osc,eq	116	71	0.61	0.04	1.244 ± 0.016	0.3768 ± 0.0020	3819 ± 8	100
13.1	e,osc,p	244	144	0.59	0.04	1.317 ± 0.015	0.3748 ± 0.0018	3811 ± 7	96
14.1	m,osc,p	120	85	0.71	0.08	1.290 ± 0.017	0.3760 ± 0.0024	3816 ± 9	97
15.1	r,h,p	341	4	0.01	<0.01	2.005 ± 0.022	0.1772 ± 0.0013	2627 ± 13	99
16.1	e,osc,p	93	52	0.56	0.08	1.321 ± 0.018	0.3773 ± 0.0036	3821 ± 15	95
17.1	e,osc,p	85	40	0.47	<0.01	1.321 ± 0.018	0.3767 ± 0.0036	3819 ± 14	95
18.1	e,osc,p	66	36	0.55	0.28	1.337 ± 0.019	0.3715 ± 0.0045	3798 ± 18	95
19.1	e,osc,p	427	225	0.53	0.22	1.476 ± 0.016	0.3295 ± 0.0017	3615 ± 8	92
20.1	r,h,p	575	3	0.01	0.09	2.046 ± 0.022	0.1762 ± 0.0013	2617 ± 13	98
20.2	m,osc,p	70	34	0.49	0.33	1.344 ± 0.020	0.3729 ± 0.0048	3803 ± 19	94
21.1	e,osc,p	94	40	0.43	0.11	1.476 ± 0.020	0.3675 ± 0.0038	3781 ± 16	88
G17/59 massive felsic schist, Felsic Volcanic formation									
1.1	m,osc,p	154	164	1.06	0.05	1.238 ± 0.033	0.3639 ± 0.0101	3766 ± 41	101
2.1	m,osc,p	56	37	0.66	0.15	1.312 ± 0.029	0.3710 ± 0.0053	3795 ± 21	96
3.1	m,osc,p	115	89	0.78	<0.01	1.243 ± 0.017	0.3727 ± 0.0029	3802 ± 12	100
4.1	m,osc,p	190	167	0.88	<0.01	1.253 ± 0.015	0.3723 ± 0.0023	3801 ± 9	99
5.1	m,osc,p	212	102	0.48	0.04	1.256 ± 0.078	0.3536 ± 0.0181	3722 ± 76	101
6.1	e,osc,p	46	28	0.60	0.27	1.290 ± 0.024	0.3696 ± 0.0063	3790 ± 25	98
7.1	e,osc,eq	183	83	0.46	0.03	1.262 ± 0.015	0.3742 ± 0.0023	3808 ± 9	99
8.1	m,osc,p	1196	1146	0.96	0.01	1.218 ± 0.013	0.3725 ± 0.0010	3802 ± 4	102
8.2	e,osc,p	833	776	0.93	<0.01	1.240 ± 0.014	0.3708 ± 0.0017	3795 ± 7	100
9.1	m,osc,eq	160	71	0.44	0.11	1.253 ± 0.016	0.3693 ± 0.0026	3788 ± 10	100
10.1	e,osc,p	201	188	0.94	0.04	1.243 ± 0.015	0.3726 ± 0.0022	3802 ± 9	100
11.1	e,osc,p	280	241	0.86	0.03	1.238 ± 0.014	0.3737 ± 0.0019	3806 ± 8	100
12.1	e,osc,p	285	163	0.57	0.02	1.254 ± 0.015	0.3740 ± 0.0018	3808 ± 7	99
13.1	e,osc,p	177	230	1.30	0.04	1.274 ± 0.019	0.3737 ± 0.0027	3806 ± 11	98
14.1	e,osc,p	594	510	0.86	0.02	1.237 ± 0.042	0.3749 ± 0.0157	3811 ± 62	100
15.1	m,osc,p	48	31	0.65	0.18	1.238 ± 0.020	0.3720 ± 0.0045	3800 ± 18	100

All uncertainties in the Table are given at 1 sigma; Site: x.y, x = grain number, y = analysis number; Grain and site character: p = prism, eq = small aspect ratio prism, m = middle of grain, e = edge of grain, r = rim overgrowth; Cathodoluminescence character: osc = oscillatory zoned, h = homogeneous; Common Pb correction: comm 206% = percentage of ^{206}Pb that is non-radiogenic, based on measured ^{204}Pb and common Pb modelled according to Cumming and Richards (1975) for likely age of zircon.

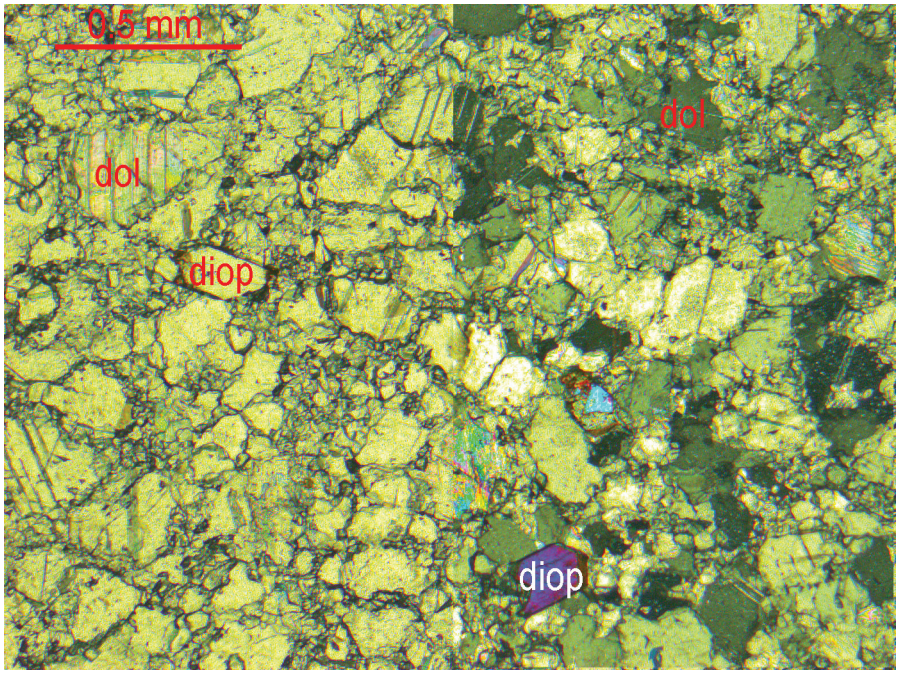

Fig. A2. Plane polarized light (left) and cross polarized light (right) photomicrograph of dolostone G12/84; dol = dolomite and diop = diopside.

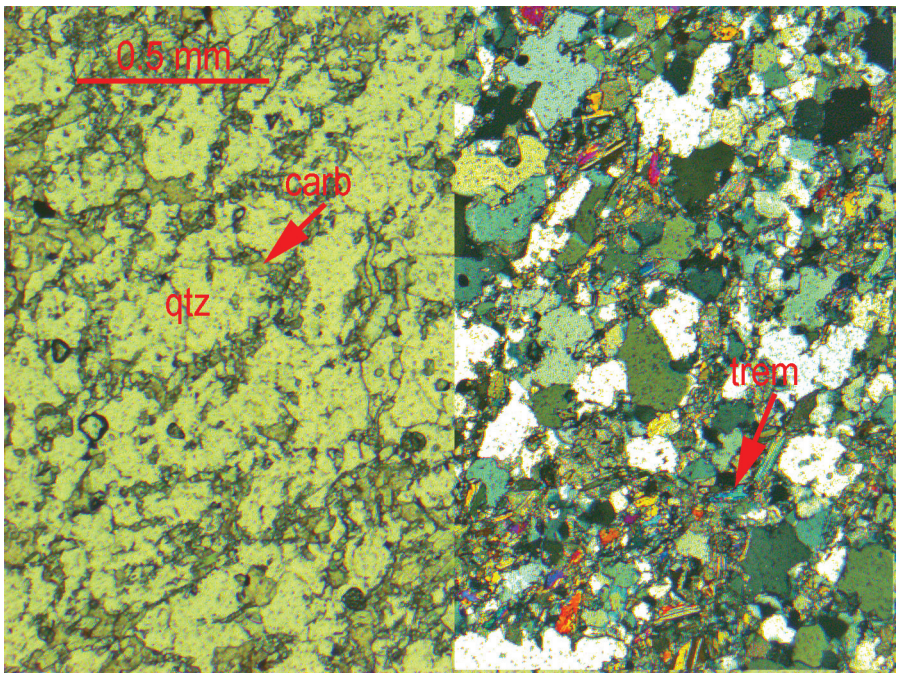

Fig. A3. Plane polarized light (left) and cross polarized light (right) photomicrographs of layered sedimentary rock G17/44B. Qtz = quartz, carb = carbonate and trem = tremolite.

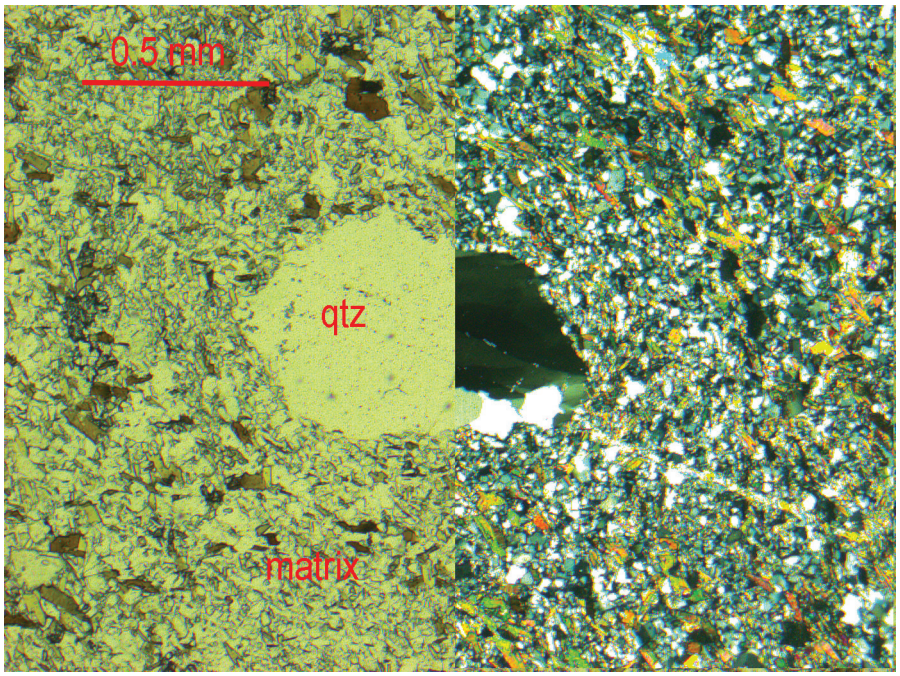

Fig. A4. Plane polarized light (left) and cross polarized light (right) photomicrographs of felsic volcanic rock G17/59. In the very fine-grained matrix is a rounded quartz grain (qtz), breaking down into a sub-grain mosaic. This is interpreted as a deformed, recrystallized corroded quartz phenocryst.

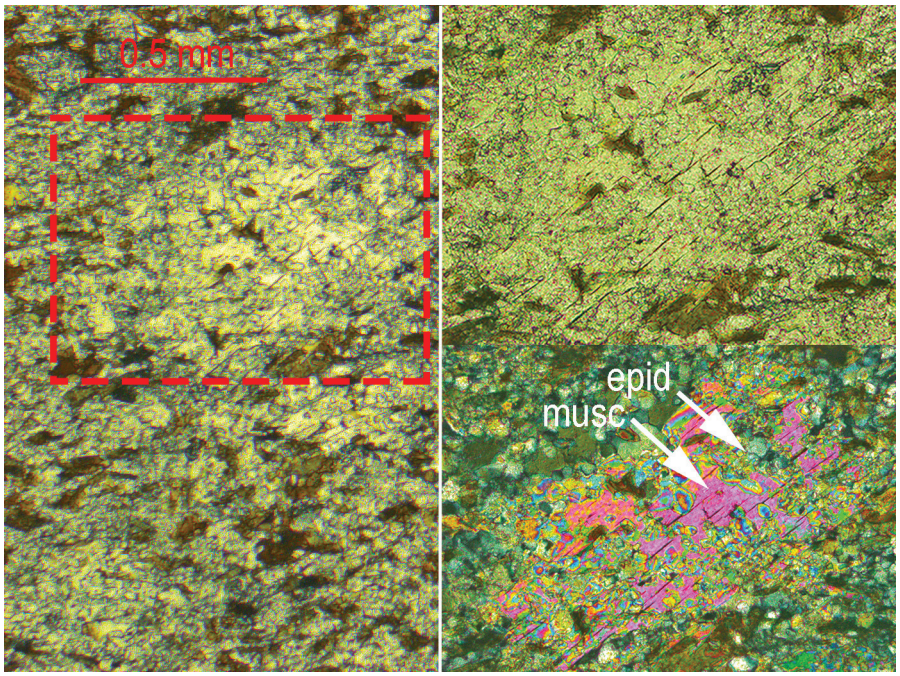

Fig. A5. Photomicrographs of felsic volcanic rock G17/59. Plane polarized light (left) and to right details of area within red box (cross polarized light, lower). The boxed object is interpreted as a plagioclase phenocryst pseudomorphed by muscovite (musc) and epidote (epid).

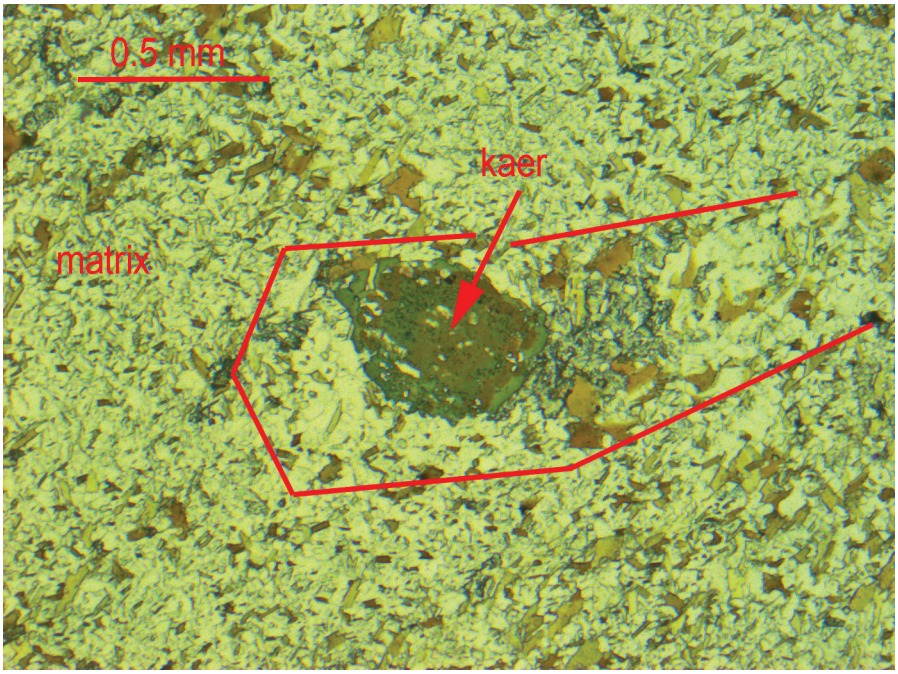

Fig. A6. Plane polarized light photomicrograph of felsic volcanic rock G17/59. Brown (kaersutite?) amphibole (kaer) phenocryst altered to green hornblende at its margins. This appears to reside in a slightly coarser-grained domain (red box) than the general matrix.

REFERENCES

Allaart, J. H., 1976, The pre-3760 m.y. old supracrustal rocks of the Isua area, central West Greenland, and the associated occurrence of quartz-banded ironstone, in Windley, B.F. editor, The Early History of the Earth: London, United Kingdom, Wiley, p. 177–189.

Appel, P. W. U., Polat, A., and Frei, R., 2009, Dacitic ocelli in mafic lavas, 3.8–3.7 Ga Isua greenstone belt, West Greenland: Geochemical evidence for partial melting of oceanic crust and magma mixing: Chemical Geology, v. 258, n. 3–4, p. 105–124, https://doi.org/10.1016/j.chemgeo.2008.09.011

Baadsgaard, H., 1976, Further U-Pb dates on zircons from the early Precambrian rocks of the Godthaabsfjord area, West Greenland: Earth and Planetary Science Letters, v. 33, n. 2, p. 261–267, https://doi.org/10.1016/0012-821X(76)90233-8

Baadsgaard, H., Nutman, A. P., and Bridgwater, D., 1986a, Geochronology and isotope variation of the early Archaean Amitsoq gneisses of the Isukasia area, southern West Greenland: Geochimica et Cosmochimica Acta, v. 50, n. 10, p. 2173–2183, https://doi.org/10.1016/0016-7037(86)90072-4

Baadsgaard, H., Nutman, A. P., Rosing, M., Bridgwater, D., and Longstaffe, F. J., 1986b, Alteration and metamorphism of Amîtsoq gneisses from the Isukasia area, West Greenland: Recommendation for isotope studies of the early crust: Geochimica et Cosmochimica Acta, v. 50, n. 10, p. 2165–2172, https://doi.org/10.1016/0016-7037(86)90071-2

Bennett, V. C., Brandon, A. D., and Nutman, A. P., 2007, Coupled ^{142}Nd-^{143}Nd isotopic evidence for Hadean mantle dynamics: Science, v. 318, n. 5858, p. 1907–1910, https://doi.org/10.1126/science.1145928

Boak, J. L., and Dymek, R. F., 1982, Metamorphism of the *ca.* 3800 Ma supracrustal rocks at Isua, West Greenland: implications for early Archaean crustal evolution: Earth and Planetary Science Letters, v. 59, n. 1, p. 155–176, https://doi.org/10.1016/0012-821X(82)90123-6

Bolhar, R., Kamber, B. S., Moorbath, S., Fedo, C. M., and Whitehouse, M. J., 2004, Characterisation of early Archaean chemical sediments by trace element signatures: Earth and Planetary Science Letters, v. 222, n. 1, p. 43–60, https://doi.org/10.1016/j.epsl.2004.02.016

Bohlar, R., Kamber, B. S., Moorbath, S., Whitehouse, M. J., and Collerson, K. D., 2005, Chemical characterization of earth's most ancient clastic metasediments from the Isua Greenstone Belt, southern West Greenland: Geochimica et Cosmochimica Acta, v. 69, p. 1553–1573, https://doi.org/10.1016/j.gca.2004.09.023

Bridgwater, D., and McGregor, V. R., 1974, Field work on the very early Precambrian rocks of the Isua area, southern West Greenland: Rapport Grønlands Geologiske Undersøgelse, v. 65, p. 49–54, https://doi.org/10.34194/rapggu.v65.7387

Collins, W. J., Van Kranendonk, M. J., and Teyssier, C., 1998, Partial convective overturn of Archaean crust in the east Pilbara Craton, Western Australia: Driving mechanisms and tectonic implications: Journal of Structural Geology, v. 20, n. 9–10, p. 1405–1424, https://doi.org/10.1016/S0191-8141(98)00073-X

Compston, W., Kinny, P. D., Williams, I. S., and Foster, J. J., 1986, The age and Pb loss behaviour of zircons from the Isua supracrustal belt as determined by ion microprobe: Earth and Planetary Science Letters, v. 80, n. 1–2, p. 71–81, https://doi.org/10.1016/0012-821X(86)90020-8

Crowley, J. L., 2003, U-Pb geochronology of 3810–3630 Ma granitoid rocks south of the Isua greenstone belt, southern West Greenland: Precambrian Research, v. 126, n. 3–4, p. 235–257, https://doi.org/10.1016/S0301-9268(03)00097-4

Crowley, J. L., Myers, J. S., and Dunning, G. R., 2002, The timing and nature of multiple 3700–3600 Ma tectonic events in intrusive rocks north of the Isua greenstone belt, southern West Greenland: GSA Bulletin, v. 114, n. 10, p. 1311–1325, https://doi.org/10.1130/0016-7606(2002)114<1311:TANOMM>2.0.CO;2

D'Andres, J., Kendrik, M. A., Bennett, V. C., and Nutman, A. P., 2019, Halogens in serpentinites from the Isua supracrustal belt, Greenland: An Eoarchaean seawater and biomass proxy?: Geochimica et Cosmochimica Acta, v. 262, p. 31–59, https://doi.org/10.1016/j.gca.2019.07.017

Dilek, Y., and Polat, A., 2008, Suprasubduction zone ophiolites and Archean tectonics: Geology, v. 36, n. 5, p. 431–432, https://doi.org/10.1130/Focus052008.1

Dymek, R. F., and Klien, C., 1988, Chemistry, petrology and origin of banded iron-formation from the 3800 Ma Isua supracrustal belt, West Greenland: Precambrian Research, v. 39, n. 4, p. 247–302, https://doi.org/10.1016/0301-9268(88)90022-8

Dymek, R. F., Brothers , S. C., and Schiffries, C. M., 1988, Petrogenesis of ultramafic metamorphic rocks from the 3800 Ma Isua supracrustal belt, West Greenland: Journal of Petrology v. 29, n. 6, p. 1353–1397, https://doi.org/10.1093/petrology/29.6.1353

Friend, C. R. L., and Nutman, A. P., 2005, Complex 3670–3500 Ma orogenic episodes superimposed on juvenile crust accreted between 3850–3690 Ma, Itsaq Gneiss Complex, southern West Greenland: Journal of Geology, v. 113, p. 375–398, https://doi.org/10.1086/430239

Friend, C. R. L., and Nutman, A. P., 2010, Eoarchean ophiolites? New evidence for the debate on the Isua supracrustal belt, southern West Greenland: American Journal of Science, v. 310, n. 9, p. 826–861, https://doi.org/10.2475/09.2010.04

Friend, C. R. L., and Nutman, A. P., 2011, Dunites from Isua, southern West Greenland: A *ca.* 3720 Ma window into subcrustal metasomatism of depleted mantle: Geology, v. 39, n. 7, p. 663–666, https://doi.org/10.1130/G31904.1

Friend, C. R. L., and Nutman, A. P., 2019, Tectono-stratigraphic terranes in Archaean gneiss complexes as evidence of plate tectonics: The Nuuk region, southern West Greenland: Gondwana Research, v. 72, p. 213–237, https://doi.org/10.1016/j.gr.2019.03.004

Friend, C. R. L., Bennett, V. C., and Nutman, A. P., 2002, Abyssal peridotites >3,800 Ma from southern West Greenland: Field relationships, petrography, geochronology, whole-rock and mineral chemistry of dunite and harzburgite inclusions in the Itsaq Gneiss Complex: Contributions to Mineralogy and Petrology, v. 143, p. 71–92, https://doi.org/10.1007/s00410-001-0332-7

Furnes, H., de Wit, M., Staudigel, H., Rosing, M., and Muehlenbachs, K., 2007, A vestige of Earth's oldest ophiolite: Science, v. 315, N. 5819, p. 1704–1707, https://doi.org/10.1126/science.1139170

Gauthiez Putallaz, L., Nutman, A., Bennett, V., and Rubatto, D., 2020, Tracking high $\delta^{18}O$ in 3.7–3.6 Ga crust: A zircon and garnet record in Isua clastic metasedimentary rocks: Chemical Geology, v. 537, https://doi.org/10.1016/j.chemgeo.2020.119474

Griffin, W. L., McGregor, V. R., Nutman, A. P., Taylor, P. N., and Bridgwater, D., 1980, Early Archaean granulite-facies metamorphism south of Ameralik: Earth and Planetary Science Letters, v. 50, n. 1, p. 59–74, https://doi.org/10.1016/0012-821X(80)90119-3

Guotana, J. M., Morishita, T., Tamura, A., Nishio, I., Tani, K., Harigane, Y., Szilas, K., and Pearson, D. G., 2019, Serpentinization and carbonation of dunites in the western part of the Isua supracrustal belt, Southwestern Greenland: JSPS-DST Japan India Forum for Advanced Study, 7–16 March, 2019, page 91.

Hiess, J., Bennett, V. C., Nutman, A. P., and Williams, I. S., 2009, *In situ* U–Pb, O and Hf isotopic compositions of zircon and olivine from Eoarchaean rocks, West Greenland: New insights to making old crust: Geochimica et Cosmochimica Acta, v. 73, n. 15, p. 4489–4516, https://doi.org/10.1016/j.gca.2009.04.019

Hoffmann, J. E., Münker, C., Næraa, T., and Rosing, M. T., 2011b, Mechanisms of Archean crust formation inferred from high-precision HFSE systematics in TTGs: Geochimica et Cosmochimica Acta, v. 75, n. 15, p. 4157–4178, https://doi.org/10.1016/j.gca.2011.04.027

Hoffmann, J. E., Münker, C., Polat, A., Rosing, M. T., and Schulz, T., 2011a, The origin of decoupled Hf–Nd isotope compositions in Eoarchean rocks from southern West Greenland: Geochimica et Cosmochimica Acta, v. 75, n. 21, p. 6610–6628, https://doi.org/10.1016/j.gca.2011.08.018

Hoffmann, J. E., Zhang, C., Moyen, J-F., and Nagel, T. J., 2019, The formation of tonalites-trondhjemite-granodiorites in early continental crust, in Van Kranendonk, M. J., Bennett, V. C., and Hoffmann, J. E., editors, Earth's Oldest Rocks (second edition): Utrecht, The Netherlands, Elsevier, p. 133–168, https://doi.org/10.1016/B978-0-444-63901-1.00007-1

Jacobsen, S. B., and Dymek, R. F., 1988. Nd and Sr isotope systematics of clastic metasediments from Isua, West Greenland: Identification of pre-3.8 Ga differentiated crustal components: Journal of Geophysical Research-Solid Earth, v. 93, n. B1, p. 338–354, https://doi.org/10.1029/JB093iB01p00338

Jenner, F. E., Bennett, V. C., Nutman, A. P., Friend, C. R. L., Norman, M. D., and Yaxley, G., 2009, Evidence for subduction at 3.8 Ga: Geochemistry of arc-like metabasalts from the southern edge of the Isua Supracrustal belt: Chemical Geology, v. 261, n. 1–2, p. 82–99, https://doi.org/10.1016/j.chemgeo.2008.09.016

Kamber, B. S., Webb, G. E., and Gallagher, M., 2014, The rare earth element signal in Archaean microbial carbonate: Information on ocean redox and biogenicity: Journal of the Geological Society, London, v. 171, n. 6, p. 745–763, https://doi.org/10.1144/jgs2013-110

Keto, L., and Kurki, J., 1967, Report on the exploration activity at Isua 1967: Kryolitselskabet Øresund A/S Prospektering report lodged as report 20024 at the Geological Survey of Denmark and Greenland.
Komiya, T., Maruyama, S., Masuda, T., Nohda, S., Hayashi, M., and Okamoto, K., 1999, Plate tectonics at 3.8–3.7 Ga: Field evidence from the Isua accretionary complex, West Greenland: The Journal of Geology, v. 107, p. 515–554, https://doi.org/10.1086/314371
Martin, H., 1986, Effect of steeper Archean geothermal gradient on geochemistry of subduction zone magmas: Geology, v. 14, n. 9, p. 753–756, https://doi.org/10.1130/0091-7613(1986)14<753:EOSAGG>2.0.CO;2
Martin, H., 1994, The Archean grey gneiss and the genesis of continental crust, in Condie, K. C., editor, Archean Crustal Evolution: Amsterdam, The Netherlands, Elsevier, Developments in Precambrian Geology, v. 11, p. 205–259, https://doi.org/10.1016/S0166-2635(08)70224-X
McDonough, W. F., and Sun, S. S., 1995, The composition of the Earth: Chemical Geology, v. 120, p. 223–253, https://doi.org/10.1016/0009-2541(94)00140-4
Moorbath, S., O'Nions, R. K., Pankhurst, R. J., Gale, N. H., and McGregor, V. R., 1972, Further rubidium-strontium age determinations on the very early Precambrian rocks of the Godthåb district, West Greenland: Nature Physical Science, v. 240, p. 78–82, https://doi.org/10.1038/physci240078a0
Myers, J. S., 2001, Protoliths of the 3.8–3.7 Ga Isua greenstone belt, West Greenland: Precambrian Research, v. 105, n. 2–4, p. 129–141, https://doi.org/10.1016/S0301-9268(00)00108-X
Nutman, A. P., 1986, The early Archaean to Proterozoic history of the Isukasia area, southern West Greenland: Bulletin Grønlands Geologiske Undersøgelse, v. 154, p. 1–80, https://doi.org/10.34194/bullggu.v154.6696
Nutman, A. P., and Bennett, V. C., 2018, The 3.9–3.6 Ga Itsaq Gneiss Complex of Greenland: Quasi-uniformitarian geodynamics towards the end of Earth's first billion years: Earth's Oldest Rocks, 2nd edition: Amsterdam, The Netherlands, p. 375–399, https://doi.org/10.1016/B978-0-444-63901-1.00017-4
Nutman, A. P., and Collerson, K. D., 1991, Very early Archean crustal-accretion complexes preserved in the North Atlantic Craton: Geology, v. 19, n. 8, p. 791–795, https://doi.org/10.1130/0091-7613(1991)019<0791:VEACAC>2.3.CO;2
Nutman, A. P., and Friend, C. R. L., 2009, New 1:20000 geological maps, synthesis and history of the Isua supracrustal belt and adjacent orthogneisses, southern West Greenland: A glimpse of Eoarchaean crust formation and orogeny: Precambrian Research, v. 172, n. 3–4, p. 189–211, https://doi.org/10.1016/j.precamres.2009.03.017
Nutman, A. P., Allaart, J. H., Bridgwater, D., Dimroth, E., and Rosing, M. T., 1984, Stratigraphic and geochemical evidence for the depositional environment of the early Archaean Isua supracrustal belt, southern West Greenland: Precambrian Research, v. 25, n. 4, p. 365–396, https://doi.org/10.1016/0301-9268(84)90010-X
Nutman, A. P., Friend, C. R. L., Kinny, P. D., and McGregor, V. R., 1993, Anatomy of an Early Archaean gneiss complex: 3900 to 3600 Ma crustal evolution in southern West Greenland: Geology, v. 21, n. 5, p. 415–418, https://doi.org/10.1130/0091-7613(1993)021<0415:AOAEAG>2.3.CO;2
Nutman, A. P., McGregor, V. R., Friend, C. R. L., Bennett, V. C., and Kinny, P. D., 1996, The Itsaq Gneiss Complex of southern West Greenland; the world's most extensive record of early crustal evolution (3900–3600 Ma): Precambrian Research, v. 78, n. 1–3, p. 1– 39, https://doi.org/10.1016/0301-9268(95)00066-6
Nutman, A. P., Bennett, V., Friend, C. R. L., and Rosing, M. T., 1997, ~3710 and ≥3790 Ma volcanic sequences in the Isua (Greenland) supracrustal belt; structural and Nd isotope implications: Chemical Geology, v. 141, n. 3–4, p. 271–287, https://doi.org/10.1016/S0009-2541(97)00084-3
Nutman, A. P., Bennett, V. C., Friend, C. R. L., and Norman, M. D., 1999, Meta-igneous (non-gneissic) tonalites and quartz-diorites from an extensive *ca.* 3800 Ma terrain south of the Isua supracrustal belt, southern West Greenland: Constraints on early crust formation: Contributions to Mineralogy and Petrology, v. 137, p. 364–388, https://doi.org/10.1007/s004100050556
Nutman, A. P., Friend, C. R. L., Bennett, V. C., and McGregor, V. R., 2000, The early Archaean Itsaq Gneiss Complex of southern West Greenland: The importance of field observations in interpreting dates and isotopic constraints for early terrestrial evolution: Geochimica et Cosmochimica Acta, v. 64, n. 17, p. 3035–3060, https://doi.org/10.1016/S0016-7037(99)00431-7
Nutman, A. P., Friend, C. R. L., and Bennett, V. C., 2002, Evidence for 3650–3600 Ma assembly of the northern end of the Itsaq Gneiss Complex, Greenland: Implication for early Archean tectonics: Tectonics, v. 21, n. 1, article 5, https://doi.org/10.1029/2000TC001203
Nutman, A. P., Friend, C. R. L., Horie, H., and Hidaka, H., 2007a, The Itsaq Gneiss Complex of southern West Greenland and the construction of Eoarchean crust at convergent plate boundaries, in Van Kranendonk, M. J., Smithies, R. H., and Bennett, V. C., editors, Earth's Oldest Rocks: Amsterdam, The Netherlands, Elsevier, Developments in Precambrian Geology, v. 15, p. 187–218, https://doi.org/10.1016/S0166-2635(07)15033-7
Nutman, A. P., Bennett, V. C., Friend, C. R. L., Horie, K., and Hidaka, H., 2007b, ~ 3850 Ma tonalites in the Nuuk region, Greenland: Geochemistry and their reworking within an Eoarchaean gneiss complex: Contributions to Mineralogy and Petrology, v. 154, p. 385–408, https://doi.org/10.1007/s00410-007-0199-3
Nutman, A. P., Friend, C. R. L., and Paxton, S., 2009, Detrital zircon sedimentary provenance ages for the Eoarchaean Isua supracrustal belt, southern West Greenland: Juxtaposition of an imbricated *ca.* 3700 Ma juvenile arc assemblage against an older complex with 3920–3800 Ma components: Precambrian Research, v. 172, n. 3–4, p. 212–233, https://doi.org/10.1016/j.precamres.2009.03.019
Nutman, A. P., Friend, C. R. L., Bennett, V. C., Wright, D., and Norman, M. D., 2010, ≥3700 Ma pre-metamorphic dolomite formed by microbial mediation in the Isua supracrustal belt (W. Greenland): Simple evidence for early life?: Precambrian Research, v. 183, n. 4, p. 725–737, https://doi.org/10.1016/j.precamres.2010.08.006

Nutman, A. P., Bennett, V. C., Friend, C. R. L., Hidaka, H., Yi, K., Lee, S. R., and Kamiichi, T., 2013, The Itsaq Gneiss Complex of Greenland: Episodic 3900 to 3660 Ma juvenile crust formation and recycling in the 3660 to 3600 Ma Isukasian orogeny: American Journal of Science, v. 313, n. 9, p. 877–911, https://doi.org/10.2475/09.2013.03

Nutman, A. P., Bennett, V. C., Chivas, A. R., Friend, C. R. L., Liu, X. M., and Dux, F. W., 2015, 3806 Ma Isua rhyolites and dacites affected by low temperature Eoarchaean surficial alteration: Earth's earliest weathering: Precambrian Research, v. 268, p. 323–338, https://doi.org/10.1016/j.precamres.2015.07.014

Nutman, A. P., Bennett, V. C., Friend, C. R. L., Van Kranendonk, M. J., and Chivas, A. R., 2016, Rapid emergence of life shown by discovery of 3,700 million year old microbial structures: Nature, v. 537, p. 535–537, https://doi.org/10.1038/nature19355

Nutman, A. P., Bennett, V. C., Friend, C. R. L., and Chivas, A.R., 2017, The Isua supracrustal belt of the North Atlantic Craton (Greenland): Spotlight on sedimentary systems with the oldest preserved sedimentary structures (~3.7, ~3.75 and ~3.8 Ga), *in* Mazumder, R., editor, Influences on Compositional Change from Source to Sink: Amsterdam, The Netherlands, Elsevier, Sediment Provenance, p. 563–592, https://doi.org/10.1016/B978-0-12-803386-9.00020-4

Nutman, A. P., Bennett, V. C., Friend, C. R. L., Van Kranendonk, M., and Chivas, A. R., 2019, Reconstruction of a 3700 Ma transgressive marine environment from Isua (Greenland): Sedimentology, stratigraphy and geochemical signatures: Lithos, v. 346–347, https://doi.org/10.1016/j.lithos.2019.105164

Nutman, A. P., Bennett, V. C., Friend, C. R. L., and Keewook, Yi, 2020, Eoarchean contrasting ultra-high-pressure to low-pressure metamorphisms (< 250 to >1000°C/GPa) explained by tectonic plate convergence in deep time: Precambrian Research, v. 344, 105770, https://doi.org/10.1016/j.precamres.2020.105770

Pearce, J. A., Harris, N. B. W., and Tindle, A. G., 1984, Trace element discrimination diagrams for the tectonic interpretation of granitic rocks: Journal of Petrology, v. 25, n. 4, p. 956–983, https://doi.org/10.1093/petrology/25.4.956

Polat, A., and Hofmann, A. W., 2003, Alteration and geochemical patterns in the 3.7–3.8 Ga Isua greenstone belt, West Greenland: Precambrian Research, v. 126, n. 3–4, p. 197–218, https://doi.org/10.1016/S0301-9268(03)00095-0

Polat, A., Hofmann, A. W., and Rosing, M. T., 2002, Boninite-like volcanic rocks in the 3.7–3.8 Ga Isua greenstone belt, West Greenland: Geochemical evidence for intra-oceanic subduction zone processes in the early Earth: Chemical Geology, v. 184, n. 3–4, p. 231–254, https://doi.org/10.1016/S0009-2541(01)00363-1

Pope, E. C., Bird, D. K., and Rosing, M. T., 2012, Isotope composition and volume of Earth's early oceans: Proceedings of the National Academy of Sciences of the United States of America, v. 109, n. 12, p. 4371–4376, https://doi.org/10.1073/pnas.1115705109

Rollinson, H., 2003, Metamorphic history suggested by garnet-growth chronologies in the Isua Greenstone Belt, West Greenland: Precambrian Research v. 126, n. 3–4, p. 181–196, https://doi.org/10.1016/S0301-9268(03)00094-9

Rosing, M. T., 1999, ^{13}C-depleted carbon microparticles in >3700 Ma sea-floor sedimentary rocks from West Greenland: Science, v. 283, n. 5402, p. 674–676, https://doi.org/10.1126/science.283.5402.674

Rosing, M. T, Rose, N. M., Bridgwater, D., and Thomsen, H. S., 1996, Earliest part of the Earth's stratigraphic record: A reappraisal of the >3.7 Ga Isua (Greenland) supracrustal sequence: Geology, v. 24, n. 1, p. 43–46, https://doi.org/10.1130/0091-7613(1996)024<0043:EPOESS>2.3.CO;2

Smithies, R. H., Champion, D. C., Van Kranendonk, M. J., 2007, The oldest well-preserved felsic volcanic rocks on Earth: Geochemical clues to the early evolution of the Pilbara Supergroup and implications for the growth of a Paleoarchean protocontinent, *in* Van Kranendonk, M. J., Smithies, R. H., and Bennett, V. C., editors, Earth's Oldest Rocks: Amsterdam, The Netherlands, Elsevier, Developments in Precambrian Geology, v. 15, p. 339–367, https://doi.org/10.1016/S0166-2635(07)15042-8

Solvang, M., 1999, An investigation of metavolcanic rocks from the eastern part of the Isua greenstone belt, Western Greenland: Copenhagen, Denmark, Geological Survey of Denmark and Greenland (GEUS) Internal Report, 62 pages.

Sossi, P. A., Eggins, S. M., Nesbitt, R. W., Nebel, O., Hergt, J. M., Campbell, I. H., O'Neill, H., St. , C., Van Kranendonk, M. J., and Davies, R. D., 2016, Petrogenesis and geochemistry of Archean komatiites: Journal of Petrology, v. 57, n. 1, p. 147–184, https://doi.org/10.1093/petrology/egw004

Steinman, G, 1905, Geologische Beobachtungenin den Alpen, II. Die schardtsche Uberfaltungstheorie und die geologische Bedeutung der Tiefseeabsätze und der ophiolotische Massengesteine: Bericht Naturforschung Gessellschaft zu Freiburg im Breigau, band 16, p. 18–67.

Stern, R. J., Reagan, M., Ishizuka, O., Ohara, Y., and Whattam, S., 2012, To understand subduction initiation, study forearc crust: To understand forearc crust, study ophiolites: Lithosphere, v. 4, n. 6, p. 469–483, https://doi.org/10.1130/L183.1

Van Kranendonk, M. J., Webb, G. E., and Kamber, B. S., 2003, Geological and trace element evidence for marine sedimentary environment of deposition and biogenicity of 3.45 Ga stromatolite carbonates in the Pilbara Craton, and support for a reducing Archean ocean: Geobiology, v. 1, n. 2, p. 91–108, https://doi.org/10.1046/j.1472-4669.2003.00014.x

Webb, A. A. G., Müller, T., Zuo, J. W., Haproff, P. J., and Ramirez-Salazar, A., 2020, A non-plate tectonic model for the Eoarchean Isua supracrustal belt: Lithosphere, v. 12, n. 1, p. 116–179, https://doi.org/10.1130/L1130.1